

Reducing orbital eccentricity of precessing black-hole binaries

Alessandra Buonanno,¹ Lawrence E. Kidder,² Abdul H. Mroué,³ Harald P. Pfeiffer,³ and Andrea Taracchini¹

¹*Maryland Center for Fundamental Physics & Joint Space-Science Institute,
Department of Physics, University of Maryland, College Park, MD 20742*

²*Center for Radiophysics and Space Research, Cornell University, Ithaca, New York, 14853*

³*Canadian Institute for Theoretical Astrophysics, University of Toronto, Toronto, Ontario M5S 3H8, Canada*

(Dated: June 1, 2011)

Building initial conditions for generic binary black-hole evolutions which are not affected by initial spurious eccentricity remains a challenge for numerical-relativity simulations. This problem can be overcome by applying an eccentricity-removal procedure which consists of evolving the binary black hole for a couple of orbits, estimating the resulting eccentricity, and then restarting the simulation with corrected initial conditions. The presence of spins can complicate this procedure. As predicted by post-Newtonian theory, spin-spin interactions and precession prevent the binary from moving along an adiabatic sequence of spherical orbits, inducing oscillations in the radial separation and in the orbital frequency. For single-spin binary black holes these oscillations are a direct consequence of monopole-quadrupole interactions. However, spin-induced oscillations occur at approximately twice the orbital frequency, and therefore can be distinguished and disentangled from the initial spurious eccentricity which occurs at approximately the orbital frequency. Taking this into account, we develop a new eccentricity-removal procedure based on the derivative of the orbital frequency and find that it is rather successful in reducing the eccentricity measured in the orbital frequency to values less than 10^{-4} when moderate spins are present. We test this new procedure using numerical-relativity simulations of binary black holes with mass ratios 1.5 and 3, spin magnitude 0.5, and various spin orientations. The numerical simulations exhibit spin-induced oscillations in the dynamics at approximately twice the orbital frequency. Oscillations of similar frequency are also visible in the gravitational-wave phase and frequency of the dominant $l = 2$, $m = 2$ mode.

PACS numbers: 04.25.D-, 04.25.dg, 04.25.Nx, 04.30.-w

I. INTRODUCTION

Over the last few years, numerical simulations of binary black holes have improved tremendously (see e.g., the recent reviews [1–3]). These simulations are now used to aid data analysts for gravitational-wave detectors in the construction of analytical templates [4–9], and in testing the efficiency of detector pipelines by injecting numerical waveforms [10].

During the gravitational-radiation driven inspiral of a binary black hole, the orbital eccentricity decreases very quickly [11, 12]. For binary black holes formed from binary stellar evolution [13] (instead of dynamical capture [14, 15]), the orbital eccentricity is expected to be essentially zero by the time the binary enters the frequency band of ground-based gravitational-wave detectors. Therefore, it is important that numerical simulations can be done for very low eccentricity binaries.

Performing black-hole simulations with very small orbital eccentricity is not easy for several reasons. Orbital parameters that result in vanishing eccentricity are only known approximately through post-Newtonian (PN) theory [16]. The translation of orbital parameters from PN theory into a complete binary black-hole initial-data set is ambiguous, because of differing coordinate systems and effects arising from solving the non-linear Einstein constraint equations [17]. And finally, early in a numerical evolution each black hole relaxes toward a steady state, affecting the black-hole masses, spins [18–20], and orbital parameters.

The complete evolution of a binary black hole is determined by its initial data. Therefore, control of orbital eccentricity has to be addressed in the construction of the initial data. The first approaches to construct low-eccentricity initial data were based on the assumption of *circular* orbits with the orbital frequency determined by the effective potential method [21–23] and the “Komar mass” ansatz [24–28]. Both methods were shown to give similar results [28]. Reference [29] presented techniques to measure eccentricity based on initial data alone. When binary black-hole evolutions became possible [30–32], it was realized that initial data constructed using the assumption of circular orbits resulted in a *spurious* orbital eccentricity of order one percent [33–35], primarily due to neglecting the radial inspiral velocity, and due to the initial relaxation of the black holes.

Two techniques are in use to achieve an orbital eccentricity smaller than what can be achieved with quasi-circular initial data. One approach [36] evolves PN equations for the trajectories of the centers of the black holes. This subsidiary evolution of ordinary differential equations is started at large initial separation, so that any spurious eccentricity due to the initial conditions dies out and the binary settles down to an inspiraling orbit with non-zero radial velocity. At the desired separation, the subsidiary evolution is stopped, the positions and velocities of the particles are read off, and are used as initial data parameters for the construction of the initial data set for the subsequent numerical evolution. This approach reduces eccentricity to about 0.002 for equal-

mass, non-spinning binaries, but is less successful for unequal masses or high spins [37].

The second approach, proposed in Ref. [34] and refined in Ref. [38], performs an iterative procedure (see also Ref. [39]). One begins with initial data with reasonably low eccentricity, e.g., quasi-equilibrium initial data or initial data utilizing PN information. One evolves this initial data for about two to three orbits, analyzes the orbit, and computes an improved initial data set with (hopefully) lower eccentricity. This procedure can be repeated until the desired degree of eccentricity is obtained.

In past applications, eccentricity removal was based on the behavior of the proper separation s between the black hole apparent horizons. For non-spinning black hole binaries [40] or binaries with spins parallel to the orbital angular momentum [20, 41], this works very well, and the eccentricity drops by about an order of magnitude with each iteration. However, when one applies this eccentricity removal procedure to *precessing* binaries, one encounters the difficulties illustrated in Fig. 1. At high eccentricity $e \gtrsim 0.01$, \dot{s} (where we indicate with a dot the derivative with respect to time) shows the expected oscillations with a period somewhat longer than the orbital period.¹ At sufficiently small eccentricity, however, the proper separation s and the radial velocity \dot{s} exhibit oscillations at *twice* the orbital frequency (or one-half the orbital period). This frequency is distinct from the frequency of oscillations caused by orbital eccentricity, and its presence makes it very hard to further reduce eccentricity based on an analysis of the proper separation s .

In this paper, we investigate these oscillations at twice the orbital frequency, and develop techniques for eccentricity removal for precessing binaries that mitigate the issues illustrated in Fig. 1. We can understand these oscillations based on PN calculations. In fact, as it was shown in Refs. [43–45], spin-spin interactions in the dynamics and spin precession, can introduce oscillations in the orbital separation and orbital frequency that prevent the binary from moving along a sequence of spherical orbits. Moreover, for single-spin binary black holes, the presence of spin-induced oscillations in the dynamics is a direct consequence of monopole-quadrupole interactions, that is of interactions of the form $m_1 S_2^2/m_2$ and $m_2 S_1^2/m_1$. It turns out that the amplitude of the *spin-induced oscillations* in the orbital frequency is half the amplitude of the oscillations in the coordinate separation. Therefore, we propose to base the iterative eccentricity removal on the orbital frequency and its time-derivative. We develop the relevant updating formulae for iterative eccentricity removal based on the (time-derivative) of the orbital frequency, and demonstrate with fully numerical simulations that iterative eccentricity removal can proceed to much smaller eccentricities $e \lesssim 10^{-4}$ that are measured in the orbital frequency.

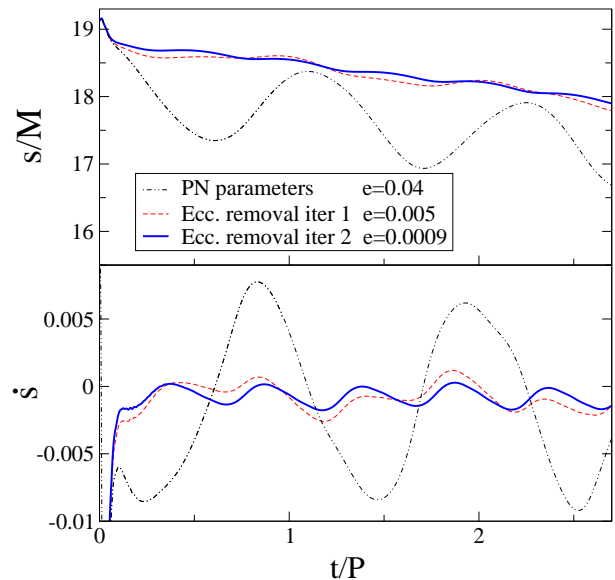


FIG. 1. Eccentricity removal based on **proper separation** applied to a *precessing* binary black hole: The horizontal axis represents time in units of the initial orbital period $P = 442M$. For eccentricity $e \gtrsim 0.01$, oscillations due to orbital eccentricity with period $\sim P$ dominate, and eccentricity removal is effective. For $e \sim 0.01$ oscillations at *one-half* the orbital period become apparent, spoiling further eccentricity removal based on \dot{s} . In this example, the mass-ratio is $m_1/m_2 = 1.5$, the larger black hole carries spin $S_1 = 0.5m_1^2$ with initial direction tangent to the orbital plane, and the smaller black hole has zero spin.

We also find that PN theory predicts spin-induced oscillations in the separation with much smaller amplitude than those visible in Fig. 1. Figure 1 utilizes the *proper separation* s between the apparent horizons along a line element joining their centers. We find that use of the *coordinate separation* between the centers of the apparent horizons instead results in much smaller oscillations. Finally, we find that the spin-induced oscillations are also present in the gravitational-wave frequency and phase, and are qualitatively reproduced by the simple PN model used here.

This paper is organized as follows. In Sec. II, we work out the spin-induced oscillations in the radial separation and orbital frequency for a PN model utilizing the Taylor-expanded PN Hamiltonian with only the lowest order PN terms responsible for the spin-induced oscillations. We also compare the obtained analytic formulae with numerical solutions of the ordinary differential equations describing a PN binary. In Sec. III, we present the new method to reduce orbital eccentricity in presence of spins. In Sec. IV, we apply our improved eccentricity-removal procedure to fully general-relativistic simulations of single and double spin binary black holes, and compare the results with the earlier eccentricity-removal procedure based on the proper horizon separation. We also investigate the presence of spin-induced oscillations in the

¹ The period of radial oscillations exceeds the orbital period because of periastron advance [42].

gauge-invariant gravitational-wave phase and frequency of a single-spin binary black hole. Finally, in Sec. V we summarize our main conclusions.

II. ECCENTRICITY AND SPIN-INDUCED OSCILLATIONS

As mentioned in the introduction, spin-spin effects and precession can induce oscillations in the orbital radial separation and frequency preventing the binary black holes from moving along an adiabatic sequence of spherical orbits. This result can be obtained in a straightforward manner in PN theory [43–45]. Here we re-analyse it in some detail using the PN Hamiltonian formalism.

As we shall see, when spins are not aligned with the initial direction of the orbital angular momentum, the spin-induced oscillations are unavoidable and their importance increases at smaller distances, since at leading order spin-spin interactions scale as $1/r^3$, where r is the binary separation. Thus, if we were to start the binary black-hole evolution at large separation with some initial orbital eccentricity, we expect that, by the time the binary reaches smaller separations, only spin-induced oscillations would be left. However, numerical-relativity simulations start the evolution at a separation where the initial orbital eccentricity is not negligible. As we shall discuss, there exists an efficient way to distinguish and disentangle the initial orbital eccentricity from the spin-induced oscillations, namely the typical frequency at which these two effects occur.

Henceforth we use natural units $G = c = 1$.

A. Eccentricity in Newtonian dynamics

Here we briefly review some useful formulae of Newtonian dynamics of eccentric orbits that we shall use below.

In the center-of-mass frame, the two-body problem reduces to a one-body problem for a particle of reduced mass $\mu = m_1 m_2 / M$, subject to the acceleration $\ddot{\mathbf{r}} = -M/r^3 \mathbf{r}$, where $M = m_1 + m_2$ is the total mass of the binary. In the Keplerian parametrization, a Newtonian orbit of eccentricity e can be described in terms of the eccentric anomaly u (see, e.g., Ref. [46])

$$u(t) - e \sin u(t) = \bar{\Omega} t, \quad (1)$$

where $\bar{\Omega} = \sqrt{M/a^3}$, a being the semi-major axis, so that

$$r(t) = \frac{\bar{r}}{1 - e^2} [1 - e \cos u(t)], \quad (2)$$

where $\bar{r} = a(1 - e^2)$. In the limit of small e we can approximate $r(t)$ using only the first harmonic, that is

$$r(t) = \bar{r} [1 - e \cos(\bar{\Omega} t)] + \mathcal{O}(e^2). \quad (3)$$

In fact, although the frequency spectrum of $r(t)$ contains all harmonics in $\bar{\Omega}$, a Fourier analysis of $r(t)$ shows

that harmonics beyond the first one are quite suppressed in presence of a small eccentricity (see, e.g., Ref. [46]). In the Keplerian parametrization the orbital frequency reads

$$\Omega(t) = \frac{\bar{\Omega} \sqrt{1 - e^2}}{[1 - e \cos u(t)]^2}, \quad (4)$$

and in the limit of small e we find

$$\Omega(t) = \bar{\Omega} [1 + 2e \cos(\bar{\Omega} t)] + \mathcal{O}(e^2). \quad (5)$$

So, in Newtonian dynamics, whenever we have an eccentricity in $r(t)$, we expect oscillations of amplitude $2e \bar{\Omega}$ at the frequency $\bar{\Omega}$ in $\Omega(t)$.

B. Two-body dynamics for spinning black holes in PN theory

We consider a binary composed of two black holes with masses m_1 and m_2 and spins \mathbf{S}_1 and \mathbf{S}_2 . The binary dynamics can be described using the spinning Taylor-expanded PN Hamiltonian. In the center-of-mass frame, the Hamiltonian depends on the canonical variables (\mathbf{r}, \mathbf{p}) which describe the motion of a particle of reduced mass μ , and on the spins \mathbf{S}_1 and \mathbf{S}_2 .

For the purposes of our analysis, it is sufficient to restrict the discussion to the Newtonian Hamiltonian, H_{Newt} , and include only the leading 1.5PN spin-orbit (SO) interaction [47], H_{SO} , and the leading 2PN spin-spin (SS) interaction [48], H_{SS} , where the SS interaction includes spin-induced monopole-quadrupole terms [49]. The Hamiltonian reads

$$H = H(\mathbf{r}, \mathbf{p}; \mathbf{S}_1, \mathbf{S}_2) = H_{\text{Newt}} + H_{\text{SO}} + H_{\text{SS}}, \quad (6)$$

where

$$H_{\text{Newt}} = \frac{\mathbf{p}^2}{2\mu} - \frac{\mu M}{r}, \quad (7)$$

$$H_{\text{SO}} = \frac{2}{r^3} \mathbf{S}_{\text{eff}} \cdot \mathbf{L}, \quad (8)$$

$$H_{\text{SS}} = \frac{\mu}{2Mr^3} [3(\mathbf{S}_0 \cdot \hat{\mathbf{n}})^2 - \mathbf{S}_0^2], \quad (9)$$

with $\mathbf{L} = \mathbf{r} \times \mathbf{p}$, $\hat{\mathbf{n}} = \mathbf{r}/|\mathbf{r}|$ and

$$\mathbf{S}_{\text{eff}} = \left(1 + \frac{3m_2}{4m_1}\right) \mathbf{S}_1 + \left(1 + \frac{3m_1}{4m_2}\right) \mathbf{S}_2, \quad (10)$$

$$\mathbf{S}_0 = \left(1 + \frac{m_2}{m_1}\right) \mathbf{S}_1 + \left(1 + \frac{m_1}{m_2}\right) \mathbf{S}_2. \quad (11)$$

For reference, we point out that \mathbf{S}_0 can be rewritten in dimensionless form as

$$\frac{\mathbf{S}_0}{M^2} = \frac{m_1}{M} \frac{\mathbf{S}_1}{m_1^2} + \frac{m_2}{M} \frac{\mathbf{S}_2}{m_2^2}. \quad (12)$$

The Hamilton equations of motion are given by

$$\dot{r}^i = \{r^i, H\} = \frac{\partial H}{\partial p_i}, \quad (13)$$

$$\dot{p}_i = \{p_i, H\} + F_i = -\frac{\partial H}{\partial r^i} + F_i, \quad (14)$$

where F_i is the radiation-reaction force. Here we follow Ref. [50] and express F_i in terms of the Newtonian energy flux $\mathcal{F}_N = 32\mu^2/(5M^2)v^{10}$ [see Eqs. (3.15), (3.27) in Ref. [50]] where for quasi-circular orbits $v = (M\Omega)^{1/3}$. Equations (13), (14) must be supplemented with the spin precession equations

$$\dot{S}_1^i = \{S_1^i, H\} = \varepsilon^{ijk} \frac{\partial H}{\partial S_1^j} S_{1k}, \quad (15)$$

$$\dot{S}_2^i = \{S_2^i, H\} = \varepsilon^{ijk} \frac{\partial H}{\partial S_2^j} S_{2k}, \quad (16)$$

where ε^{ijk} is the Levi-Civita symbol in flat spacetime. The non-spinning conservative part of the dynamics together with the lowest-order SO interactions allows the existence of spherical orbits [$r(t)=\text{const.}$] [49]. In fact, if we consider $H = H_{\text{Newt}} + H_{\text{SO}}$, it is straightforward to show that the Hamiltonian is a spherically symmetric function that depends *only* on the radial separation and its conjugated momentum, i.e., $H = H(r, p_r)$. This happens because the other degrees of freedom are constrained by the constants of motion: \mathbf{L}^2 and $\mathbf{S}_{\text{eff}} \cdot \mathbf{L}$. More explicitly

$$H(r, p_r) = \frac{1}{2\mu} \left(p_r^2 + \frac{\mathbf{L}^2}{r^2} \right) - \frac{\mu M}{r} + \frac{2}{r^3} \mathbf{S}_{\text{eff}} \cdot \mathbf{L}. \quad (17)$$

Imposing that at $t = 0$, $r = r_0 = \text{const.}$, we have

$$[\dot{r}]_0 = \left[\frac{\partial H}{\partial p_r} \right]_0 = \left[\frac{p_r}{\mu} \right]_0 = 0 \quad (18)$$

and to have a stable spherical orbit we have to require also that $[\dot{p}_r]_0 = 0$, hence

$$\begin{aligned} [\dot{p}_r]_0 &= \left[-\frac{\partial H}{\partial r}(r, p_r = 0) \right]_0 \\ &= \left[\frac{\mathbf{L}^2}{\mu r^3} - \frac{\mu M}{r^2} + \frac{6}{r^4} \mathbf{S}_{\text{eff}} \cdot \mathbf{L} \right]_0 = 0. \end{aligned} \quad (19)$$

Choosing properly \mathbf{L}^2 and $\mathbf{S}_{\text{eff}} \cdot \mathbf{L}$ to satisfy Eq. (19), we obtain spherical orbits. However, once SS interactions are included, this is no longer true, since \mathbf{L}^2 and $\mathbf{S}_{\text{eff}} \cdot \mathbf{L}$ are no longer constants of motion. Therefore, we must expect oscillations induced by SS terms in the radial separation and orbital frequency about their average values.

C. Oscillations induced by leading SS interactions: conservative dynamics

In this section, we investigate the behavior of the radial separation r and of the orbital frequency Ω at 2PN

order for the conservative non-spinning dynamics. While doing so, we will also assume a negligible precession of the spins and of the orbital plane, since it takes place on a longer timescale than the effects we are interested in. Henceforth, we follow the method outlined in Appendix B of Ref. [45].

As a first step, we restrict ourselves to the case in which radiation-reaction is not present (i.e., $F_i = 0$). As discussed earlier, the presence of SS terms prevents r and Ω from being constant. Thus, we write [45]

$$r(t) = \bar{r} + \delta r(t), \quad \Omega(t) = \bar{\Omega} + \delta \Omega(t), \quad (20)$$

where the bar stands for time-average $\langle \dots \rangle$ over one orbital period; hence, by definition, $\langle \delta r(t) \rangle = \langle \delta \Omega(t) \rangle = 0$. Our goal is to determine the equations that the oscillations $\delta r(t)$ and $\delta \Omega(t)$ must obey at 2PN order. For convenience, we decompose vectors with respect to the triad defined by

$$\hat{\mathbf{n}} = \frac{\mathbf{r}}{r}, \quad \hat{\mathbf{L}}_N = \frac{\mathbf{r} \times \dot{\mathbf{r}}}{|\mathbf{r} \times \dot{\mathbf{r}}|}, \quad \hat{\boldsymbol{\lambda}} = \hat{\mathbf{L}}_N \times \hat{\mathbf{n}}. \quad (21)$$

This triad is such that $\hat{\mathbf{n}}$ and $\hat{\boldsymbol{\lambda}}$ are in the instantaneous orbital plane, while $\hat{\mathbf{L}}_N$ is orthogonal to it. In the instantaneous orbital plane, we have the velocity

$$\mathbf{v} = \dot{\mathbf{r}} = \dot{r} \hat{\mathbf{n}} + \Omega r \hat{\boldsymbol{\lambda}}, \quad (22)$$

and the acceleration

$$\mathbf{a} = a_{\text{rad}} \hat{\mathbf{n}} + a_{\text{tan}} \hat{\boldsymbol{\lambda}} + a_{\perp} \hat{\mathbf{L}}_N, \quad (23)$$

with

$$a_{\text{rad}} = \hat{\mathbf{n}} \cdot \ddot{\mathbf{r}} = \ddot{r} - r \Omega^2, \quad (24)$$

$$a_{\text{tan}} = \hat{\boldsymbol{\lambda}} \cdot \ddot{\mathbf{r}} = \frac{1}{r} \frac{d}{dt} (r^2 \Omega), \quad (25)$$

and

$$a_{\perp} = \hat{\mathbf{L}}_N \cdot \ddot{\mathbf{r}} = r \Omega \left(\hat{\boldsymbol{\lambda}} \cdot \frac{d\hat{\mathbf{L}}_N}{dt} \right). \quad (26)$$

For future reference, we define the projection of \mathbf{S}_0 on the instantaneous orbital plane

$$\mathbf{S}_{0\perp} = \mathbf{S}_0 - \mathbf{S}_0 \cdot \hat{\mathbf{L}}_N. \quad (27)$$

Note that Eq. (22) implicitly defines Ω . We have $\Omega = (\dot{\mathbf{r}} \cdot \hat{\boldsymbol{\lambda}})/r$. We need the acceleration $\ddot{\mathbf{r}}$ so we take a time derivative of Eq. (13) and substitute Eq. (14) into that. We note that the Newtonian orbital angular momentum can be written as

$$\mathbf{L}_N = \mu \Omega r^2 \hat{\mathbf{L}}_N, \quad (28)$$

while the orbital angular momentum $\mathbf{L} = \mathbf{r} \times \mathbf{p}$ can be obtained from the Hamilton equation (13), that is to say

$$\dot{\mathbf{r}} = \frac{\mathbf{p}}{\mu} + \frac{2}{r^3} (\mathbf{S}_{\text{eff}} \times \mathbf{r}), \quad (29)$$

so that

$$\mathbf{L} = \mathbf{L}_N - \frac{2\mu}{r} [\mathbf{S}_{\text{eff}} - \hat{\mathbf{n}} (\mathbf{S}_{\text{eff}} \cdot \hat{\mathbf{n}})]. \quad (30)$$

Since we want to work consistently at 2PN order, we replace \mathbf{L} with Eq. (30) whenever it shows up in our calculations and drop higher PN terms. It is then straightforward to compute the radial component of the acceleration

$$a_{\text{rad}} = -\frac{M}{r^2} \left\{ 1 - \frac{2}{\mu M r^2} (\mathbf{S}_{\text{eff}} \cdot \hat{\mathbf{L}}_N) - \frac{3}{2M^2 r^2} [3(\mathbf{S}_0 \cdot \hat{\mathbf{n}})^2 - \mathbf{S}_0^2] \right\} \quad (31)$$

Since the leading-order spin acceleration is of 1.5PN order, we assume that the radial oscillations scale at least as $\dot{r} = \mathcal{O}(3)$.² Hence, when computing the tangential component of the acceleration, at 2PN accuracy, we set $\dot{r} = 0$ ($\mathbf{v} = r \Omega \hat{\boldsymbol{\lambda}}$) and $p_r = 0$ in every term coming from SO or SS interactions. Moreover, we also neglect any term depending on the time derivative of the spin in a_{tan} , since it is of higher PN order. This means that we are implicitly assuming that the spins are constant. At 2PN order, we are left with

$$a_{\text{tan}} = -\frac{3}{M r^4} (\mathbf{S}_0 \cdot \hat{\mathbf{n}}) (\mathbf{S}_0 \cdot \hat{\boldsymbol{\lambda}}). \quad (32)$$

Combining Eq. (25) with Eq. (32), we solve for $r^2 \Omega$ by integrating Eq. (32). In doing that, we assume that r and Ω in the right-hand side of Eq. (32) are constants, as their time derivatives are at least $\mathcal{O}(3)$, and also the spins are constants, that is they do not precess. Thus, under those assumptions, the time evolution of the triad $\{\hat{\mathbf{n}}, \hat{\boldsymbol{\lambda}}, \hat{\mathbf{L}}_N\}$ is such that $\hat{\mathbf{n}}$ and $\hat{\boldsymbol{\lambda}}$ swipe the orbital plane at a frequency $\bar{\Omega}$ while $\hat{\mathbf{L}}_N$ stays fixed:

$$\hat{\mathbf{n}}(t) = \cos(\bar{\Omega}t) \hat{\mathbf{n}}_0 + \sin(\bar{\Omega}t) \hat{\boldsymbol{\lambda}}_0, \quad (33)$$

$$\hat{\boldsymbol{\lambda}}(t) = -\sin(\bar{\Omega}t) \hat{\mathbf{n}}_0 + \cos(\bar{\Omega}t) \hat{\boldsymbol{\lambda}}_0, \quad (34)$$

$$\hat{\mathbf{L}}_N(t) = \hat{\mathbf{L}}_{N0}, \quad (35)$$

where $\hat{\mathbf{n}}_0 = \hat{\mathbf{n}}(0)$, $\hat{\boldsymbol{\lambda}}_0 = \hat{\boldsymbol{\lambda}}(0)$ and $\hat{\mathbf{L}}_{N0} = \hat{\mathbf{L}}_N(0)$, and also

$$\dot{\hat{\mathbf{n}}} = \bar{\Omega} \hat{\boldsymbol{\lambda}} \quad \dot{\hat{\boldsymbol{\lambda}}} = -\bar{\Omega} \hat{\mathbf{n}}. \quad (36)$$

Moreover, since we assume that the spins remain constant, we formally set $\mathbf{S}_1(t) = \mathbf{S}_1(0)$ and $\mathbf{S}_2(t) = \mathbf{S}_2(0)$, so in what follows $\mathbf{S}_0 = \mathbf{S}_0(0)$ and $\mathbf{S}_{\text{eff}} = \mathbf{S}_{\text{eff}}(0)$. By inserting Eqs. (20) into Eqs. (31) and (32), one obtains a pair of coupled differential equations:

$$\begin{aligned} \delta \ddot{r} - \bar{r} \bar{\Omega}^2 - \bar{\Omega}^2 \delta r - 2\bar{r} \bar{\Omega} \delta \Omega = & -\frac{M}{\bar{r}^2} \times \\ & \times \left\{ 1 - \frac{2\bar{\Omega}}{M} (\mathbf{S}_{\text{eff}} \cdot \hat{\mathbf{L}}_N) \right. \\ & \left. - \frac{3}{2M^2 \bar{r}^2} [3(\mathbf{S}_0 \cdot \hat{\mathbf{n}})^2 - \mathbf{S}_0^2] \right\} + 2\frac{M}{\bar{r}^3} \delta r \end{aligned} \quad (37)$$

and

$$2\bar{\Omega} \bar{r} \delta r + \bar{r}^2 \delta \Omega = k - \frac{3}{2M \bar{\Omega} \bar{r}^3} (\mathbf{S}_0 \cdot \hat{\mathbf{n}})^2. \quad (38)$$

Here, k is an integration constant and, again, in the right-hand-side of the above equations we keep only terms through 2PN order. To fix k we time-average the above equations. We have

$$\begin{aligned} \langle (\mathbf{S}_0 \cdot \hat{\mathbf{n}}(t))^2 \rangle &= S_{0i} S_{0j} \langle n^i(t) n^j(t) \rangle = \\ &= S_{0i} S_{0j} \frac{1}{2} \left(\delta^{ij} - \hat{L}_{N0}^i \hat{L}_{N0}^j \right) = \frac{1}{2} \left[\mathbf{S}_0^2 - (\mathbf{S}_0 \cdot \hat{\mathbf{L}}_{N0})^2 \right], \end{aligned} \quad (39)$$

obtaining

$$k = \frac{3}{4M \bar{\Omega} \bar{r}^3} \left[\mathbf{S}_0^2 - (\mathbf{S}_0 \cdot \hat{\mathbf{L}}_{N0})^2 \right]. \quad (40)$$

Taking the time average of Eq. (37), we derive the following modified version of Kepler's law relating \bar{r} and $\bar{\Omega}$

$$\bar{\Omega}^2 = \frac{M}{\bar{r}^3} - \frac{2\bar{\Omega}}{\bar{r}^3} \mathbf{S}_{\text{eff}} \cdot \hat{\mathbf{L}}_{N0} + \frac{3}{4M \bar{r}^5} \left[3(\mathbf{S}_0 \cdot \hat{\mathbf{L}}_{N0})^2 - \mathbf{S}_0^2 \right]. \quad (41)$$

We decouple Eq. (37) from Eq. (38), then we use Eq. (41). Since we expect that $\delta r = \mathcal{O}(4)$, we find that at 2PN order

$$\delta \ddot{r} + \bar{\Omega}^2 \delta r = -\frac{3}{4M \bar{r}^4} \left[(\mathbf{S}_0 \cdot \hat{\boldsymbol{\lambda}})^2 - (\mathbf{S}_0 \cdot \hat{\mathbf{n}})^2 \right], \quad (42)$$

in agreement with Eq. (B13) of Ref. [45]. The solution of the homogeneous equation is simply

$$\delta r(t)_{\text{hom}} = A_r \cos(\bar{\Omega}t + \varphi_r), \quad (43)$$

where A_r and φ_r are fixed by the initial conditions. Equation (43) describes possible oscillations due to the initial eccentricity of the orbit. This eccentricity occurs at the average orbital frequency and in principle can be removed as long as quasi-circular initial conditions are enforced. Note that Eq. (43) is also consistent with the Newtonian result of Eq. (3).³ It is worth noting that Eq. (3) was derived as an expansion for a small eccentricity e , while in this section we never explicitly referred to e at all. As a matter of fact, we are dealing with quasi-circular orbits here, so that consistency between Eqs. (3) and (43) should be expected.

On the other hand, the spin-induced oscillations are described by the particular solution of Eq. (42) which reads

$$\delta r_{\text{part}}(t) = \frac{1}{4M^2 \bar{r}} \left[(\mathbf{S}_0 \cdot \hat{\boldsymbol{\lambda}}(t))^2 - (\mathbf{S}_0 \cdot \hat{\mathbf{n}}(t))^2 \right]. \quad (44)$$

² We denote the nPN order as $\mathcal{O}(2n)$

³ Note that Eq. (3) does not depend on φ because in Eq. (2) the radial separation at $t = 0$ is picked to be equal to the semi-major axis.

These oscillations are a signature of SS interactions since they depend on \mathbf{S}_0 , which enters H_{SS} . Once we know $\delta r = \delta r_{\text{hom}} + \delta r_{\text{part}}$, we solve Eq. (38) for $\delta\Omega$. Similarly to what we found above, the homogeneous solution accounts for the initial conditions, while the particular solution accounts for the oscillations induced by SS effects.

$$\delta\Omega_{\text{part}}(t) = \frac{\bar{\Omega}}{4M^2\bar{r}^2} \left[(\mathbf{S}_0 \cdot \hat{\lambda}(t))^2 - (\mathbf{S}_0 \cdot \hat{n}(t))^2 \right]. \quad (45)$$

The above equation is also consistent with the Newtonian result of Eq. (5).

So far, we have assumed the nonspinning dynamics to be Newtonian. If we included nonspinning PN corrections through 3PN order in the Hamiltonian, we would still find the particular solutions (44) and (45), but in this case the oscillations would occur at a frequency which will differ from Eq. (41) because of nonspinning PN corrections.

Using the previous results, it is straightforward to compute the time derivatives of the oscillations $\delta\dot{r}$, Eq. (44), and $\delta\dot{\Omega}$, Eq. (45). They read

$$\delta\dot{r}(t) = B_r \sin(\bar{\Omega}t + \varphi_r) - \frac{\bar{\Omega}}{M^2\bar{r}} (\mathbf{S}_0 \cdot \hat{n}(t)) (\mathbf{S}_0 \cdot \hat{\lambda}(t)), \quad (46)$$

$$\delta\dot{\Omega}(t) = B_\Omega \sin(\bar{\Omega}t + \varphi_\Omega) - \frac{\bar{\Omega}^2}{M^2\bar{r}^2} (\mathbf{S}_0 \cdot \hat{n}(t)) (\mathbf{S}_0 \cdot \hat{\lambda}(t)). \quad (47)$$

We note that when the spins are initially aligned or antialigned to $\hat{\mathbf{L}}_{\text{N}0}$, the SS oscillations disappear, since in this situation \mathbf{S}_0 remains perpendicular to $\hat{\mathbf{n}}$ and $\hat{\lambda}$ throughout the evolution. We see that for both quantities the time dependence of the SS term is

$$(\mathbf{S}_0 \cdot \hat{n}(t)) (\mathbf{S}_0 \cdot \hat{\lambda}(t)) = C \sin(2\bar{\Omega}t + \gamma), \quad (48)$$

where

$$C = \frac{(\mathbf{S}_0 \cdot \hat{n}_0)^2 + (\mathbf{S}_0 \cdot \hat{\lambda}_0)^2}{2} \quad (49)$$

and γ satisfies

$$\begin{aligned} \sin \gamma &= \frac{1}{2} \sin(2\alpha), \\ \cos \gamma &= -\frac{1}{2} \cos(2\alpha), \end{aligned} \quad (50)$$

with $\cos \alpha = \hat{\mathbf{S}}_{0\perp} \cdot \hat{\mathbf{n}}_0$. Thus, the spin-induced oscillations occur at *twice* the average orbital frequency, and they can be neatly disentangled from the eccentricity induced by initial conditions which occurs at the average orbital frequency.

Moreover, the amplitude of spin-induced oscillations is quite small. To place their amplitude into perspective, consider a binary with orbital eccentricity e . Taking a time-derivative of Eqs. (2) and (5), and comparing to Eqs. (46) and (47) we find $B_r = \bar{r}\bar{\Omega}e$ and $B_\Omega = 2\bar{\Omega}^2e$.

Equating the amplitudes of the spin-induced oscillations with the amplitude of the eccentricity-induced term, we see that spin-induced oscillations dominate only for eccentricities

$$e < \begin{cases} \frac{1}{2} \frac{S_{0\perp}^2}{M^4} \left(\frac{\bar{r}}{M} \right)^{-2} & \text{for } \delta\dot{r}, \\ \frac{1}{4} \frac{S_{0\perp}^2}{M^4} \left(\frac{\bar{r}}{M} \right)^{-2} & \text{for } \delta\dot{\Omega}. \end{cases} \quad (51)$$

Numerical binary black-hole simulations typically start at a separation $\bar{r}/M \approx 15$, and in that case, spin-induced oscillations will dominate $\delta\dot{r}$ and $\delta\dot{\Omega}$ only for $e < 0.002 S_{0\perp}^2/M^4$ and for $e < 0.001 S_{0\perp}^2/M^4$, respectively. For maximally spinning black holes with least-favorable spin orientations, $S_{0\perp}/M^2 = 1$, so that even in this case spin-induced oscillations become relevant only at eccentricities of $\lesssim 0.001$. For smaller spins, their effect is still smaller. We note that spin-induced oscillations do affect $\delta\dot{\Omega}$ somewhat less than $\delta\dot{r}$, indicating that eccentricity-removal based on the orbital frequency will be preferable.

Let us notice that were we including the precession of the spins, the characteristic frequency at which the spin-induced oscillations occur would change. This can easily be seen if we assume that the precession is mainly due to SO effects, with \mathbf{S}_1 and \mathbf{S}_2 precessing about $\hat{\mathbf{L}}_{\text{N}}$ at frequencies Ω_1 and Ω_2 . In this case, using Eqs. (15), (16), we derive

$$\Omega_1 = \frac{2\mu\bar{\Omega}}{\bar{r}} \left(1 + \frac{3m_2}{4m_1} \right), \quad (52)$$

$$\Omega_2 = \frac{2\mu\bar{\Omega}}{\bar{r}} \left(1 + \frac{3m_1}{4m_2} \right). \quad (53)$$

If in Eqs. (48) (49) and (50), we let \mathbf{S}_0 precess, we obtain that oscillations occur at frequencies given by linear combinations of $\bar{\Omega}$, Ω_1 and Ω_2 , namely $2\bar{\Omega} - \Omega_1 - \Omega_2$, $2(\bar{\Omega} - \Omega_1)$ and $2(\bar{\Omega} - \Omega_2)$. For the binary black-hole evolutions considered in this paper, $\Omega_{1,2} \ll \bar{\Omega}$, so the spin-induced oscillations occur at the frequency $2\bar{\Omega}$.

Lastly, the results of this section could be extended to higher PN orders by including next-to-leading SO terms (2.5PN order [51–54]) and SS terms (3PN order [55–60]).

D. Oscillations induced by leading SS terms: inspiraling dynamics

In this section we compare the approximate analytical predictions for $\delta\dot{r}$ and $\delta\dot{\Omega}$ with the results obtained by numerically integrating the Hamilton equations (13) and (14), including the radiation reaction force F_i . Since we actually want to extract the spin-induced oscillations, we need to remove the homogeneous part which is due to the eccentricity introduced by the initial conditions. In fact, in the presence of radiation-reaction the initial radial velocity has to be carefully chosen to guarantee that the binary moves along a quasi-adiabatic sequence

of spherical orbits, progressively shrinking. Those initial conditions have been worked out in the analytical PN dynamics at post-circular [61] and post-post-circular [62] orders. However, those initial conditions become more and more approximate if we start the evolution of the Hamilton equations at smaller and smaller separations. Moreover, from the study of the conservative dynamics in Sec. II C, we understood that because of SS interactions it is impossible to have spherical orbits. To remove the oscillations at a frequency $\bar{\Omega}$ (the homogeneous part), we perform a fit of the data with a function

$$f_{\text{oscill}}(t; B_{\text{fit}}, \omega_{\text{fit}}, \varphi_{\text{fit}}) = B_{\text{fit}} \sin(\omega_{\text{fit}} t + \varphi_{\text{fit}}); \quad (54)$$

where ω_{fit} is close to $\bar{\Omega}$. We subtract the fitted function f_{oscill} from the raw data sample, obtaining a residual that oscillates at a frequency $2\bar{\Omega}$, superimposed to the smooth numerical inspiral. The reason why we need to fit also the frequency ω_{fit} is that there is an ambiguity as to what value we use for $\bar{\Omega}$. In principle, this value should be the average orbital frequency, but a priori we can only use the initial value $\Omega_0 = \Omega(0)$ because we do not have an analytic prediction for $\bar{\Omega}$. This is also true for the value of \bar{r} , which we replace with $r_0 = r(0)$ throughout. We want to compare these residuals with analytical predictions based on Eqs. (46) and (47). We use the expression of the Newtonian flux to derive the effect of the radiation reaction (RR) on the two quantities \dot{r} and $\dot{\Omega}$. Within the context of Newtonian dynamics, we have

$$\dot{r}_{\text{RR}}(t) = -\frac{64}{5} \mu M^2 \left(r_0^4 - \frac{256}{5} \mu M^2 t \right)^{-3/4}, \quad (55)$$

where $r_0 = r(0)$ and

$$r_{\text{RR}}(t) = \left(r_0^4 - \frac{256}{5} \mu M^2 t \right)^{1/4}. \quad (56)$$

A similar expression can be found also for $\dot{\Omega}_{\text{RR}}$. Considering that in a quasi-circular inspiral

$$\frac{\dot{r}_{\text{RR}}}{r_{\text{RR}}} = -\frac{2}{3} \frac{\dot{\Omega}_{\text{RR}}}{\Omega_{\text{RR}}} \quad (57)$$

and $r_{\text{RR}}^3 \Omega_{\text{RR}}^2 = M$, we find

$$\dot{\Omega}_{\text{RR}}(t) = -\frac{3}{2} M^{1/2} \frac{\dot{r}_{\text{RR}}(t)}{r_{\text{RR}}^{5/2}(t)}. \quad (58)$$

Therefore our analytical predictions will be given by

$$\dot{r}_{\text{pred}}(t) = \dot{r}_{\text{RR}}(t) + \delta \dot{r}_{\text{part}}(t) \quad (59)$$

$$\dot{\Omega}_{\text{pred}}(t) = \dot{\Omega}_{\text{RR}}(t) + \delta \dot{\Omega}_{\text{part}}(t), \quad (60)$$

where $\delta \dot{r}_{\text{part}}(t)$ and $\delta \dot{\Omega}_{\text{part}}(t)$ are given by the second term in the RHS of Eqs. (46) and (47).

Figure 2 shows the results for a particular black-hole binary with mass ratio $q = m_2/m_1 = 2$ and maximal spin magnitudes $|\mathbf{S}_1|/m_1^2 = |\mathbf{S}_2|/m_2^2 = 1$. In these plots

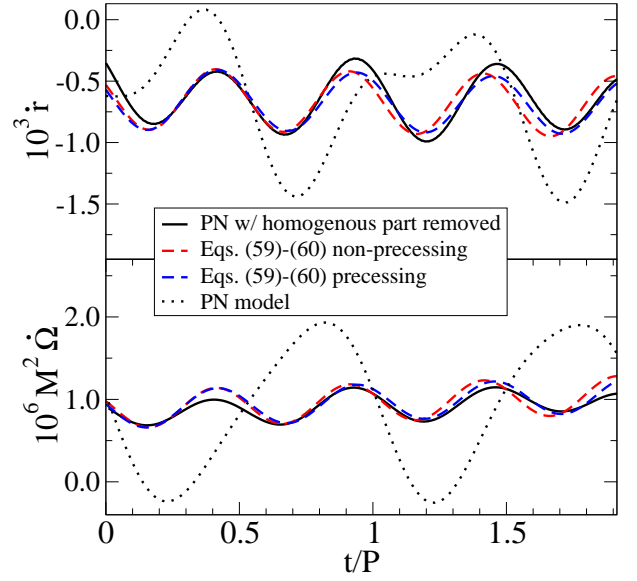


FIG. 2. Spin induced oscillations in PN model. We compare two PN calculations of spin-induced oscillations. The dashed lines are the predictions from Eqs. (59) and (60), with the two lines differing by whether $\hat{\mathbf{L}}_N$ is held constant (“non-precessing”) or evolving (“precessing”). The solid line represents a solution of the full PN equations of motions, with the homogenous oscillations fitted and subtracted. (Here, mass-ratio $q = 2$, with maximal spins of initial orientations ($\theta_1 = \pi/3, \phi_1 = 0$) and ($\theta_2 = 2\pi/3, \phi_2 = \pi/3$) at the initial orbital frequency $M\Omega_0 = 0.015$, that is an average initial orbital period $P = 418M$, and the dotted curve represents the solutions of the PN model including inspiral motion).

the initial orbital frequency is $\Omega_0 M = 0.015$ which corresponds to a period $P = 418M$. As can be seen, the raw data (dotted lines) are dominated by the eccentricity at the orbital frequency, while the residuals (solid lines) oscillate at twice the orbital frequency, as expected. As far as the amplitude of the residual oscillations is concerned, we see that it is compatible with that of the predictions computed using Eqs. (59), (60), even though the agreement is not striking (red dashed lines, called non-precessing). In fact, we find that the effectiveness of the removal procedure of the homogeneous part is deeply affected by the value of ω_{fit} . Numerical studies have shown that differences of a few percent on ω_{fit} can completely alter the residuals. Tweaking by hand the value of ω_{fit} instead of using the best fit value can lead to a much better agreement on the amplitudes, at least for the first cycle. Note that in Fig. 2 no such ad hoc tweaking is used. Also, the fact that the predictions quickly get out of phase with respect to the residuals is mainly due to the assumption made in Sec. II C of keeping the spins constant or non-precessing, that is using the evolution of the triad $\{\hat{\mathbf{n}}, \hat{\boldsymbol{\lambda}}, \hat{\mathbf{L}}_N\}$ specified by Eqs. (33)–(35). By contrast better phase agreement can be obtained numerically if we use the time-evolution of the spins and of the reference triad (blue dashed lines, called precessing)

or analytically if we had considered a reference triad in which the precession of the orbital plane and spins were taken into account.

Another interesting feature is the relative importance of the spin-induced oscillations with respect to the eccentricity induced by the initial conditions. Both types of oscillations are showing up in the raw data of \dot{r} , while in the case of $\dot{\Omega}$ we only see the oscillations due to the initial conditions. This can be explained by our analytical predictions. Using Eqs. (2), (5), we write for the eccentricity

$$e_r^{\text{NS}} = \frac{|B_r|}{\bar{r}\bar{\Omega}} \quad \text{or} \quad e_{\Omega}^{\text{NS}} = \frac{|B_{\Omega}|}{2\bar{\Omega}^2}, \quad (61)$$

where B_r and B_{Ω} are the amplitudes of the oscillations of the homogeneous solutions. We want to keep distinct notations for \dot{r} and $\dot{\Omega}$, even though at Newtonian level $e_r^{\text{NS}} = e_{\Omega}^{\text{NS}} = e$ and therefore $|B_r| = \bar{r}|B_{\Omega}|/2\bar{\Omega}$. If we now call C_r and C_{Ω} the SS amplitudes, namely

$$C_r = -\frac{\bar{\Omega}C}{M^2\bar{r}}, \quad C_{\Omega} = -\frac{\bar{\Omega}^2C}{M^2\bar{r}^2}, \quad (62)$$

we parametrize the spin-induced oscillations in terms of a spin-induced “eccentricity”,

$$e_r^{\text{SS}} = \frac{|C_r|}{\bar{r}\bar{\Omega}} = \frac{|C|}{M^2\bar{r}^2}, \quad e_{\Omega}^{\text{SS}} = \frac{|C_{\Omega}|}{2\bar{\Omega}^2} = \frac{|C|}{2M^2\bar{r}^2}. \quad (63)$$

We have that the relative ratio is

$$\frac{e_{\Omega}^{\text{SS}}}{e_r^{\text{SS}}} = \frac{1}{2}, \quad (64)$$

so it is expected that the significance of the spin-induced oscillations is smaller for $\dot{\Omega}$.

III. ITERATIVE ECCENTRICITY REMOVAL IN PRESENCE OF SPINS

In the preceding sections, we showed that the PN Hamiltonian with leading SS terms predicts oscillations with two distinct periods: the orbital period, with amplitude and phase depending on initial conditions that can genuinely be associated with orbital eccentricity; and half the orbital period, independent of the initial conditions and caused by spin-spin couplings. We furthermore showed that these spin-induced oscillations are suppressed in $\dot{\Omega}$ as compared to \dot{r} [see, e.g., Eq. (64)].

Our task is to find initial conditions that remove or at least minimize the oscillations caused by eccentricity. As in earlier work, we shall begin with some trial initial conditions, evolve the binary for about two orbits, analyze the motion of the black holes, and then correct the initial conditions. To exploit this suppression of spin-induced oscillations in $\dot{\Omega}$, we will derive updating formulae based on $\dot{\Omega}$.

A. Updating formulae

The basis for the updating formulae are the Newtonian expressions for distance r and orbital frequency Ω (Eqs. (3) and (5))

$$r_N(t) = \bar{r} [1 - e \sin \phi(t)], \quad (65)$$

$$\Omega_N(t) = \bar{\Omega} [1 + 2e \sin \phi(t)], \quad (66)$$

where $\phi(t)$ is the phase of the radial oscillations. General relativistic periastron advance will cause $\phi(t)$ to deviate from the orbital phase. Taking a time-derivative, we find

$$\dot{r}_N = -\bar{r} e \omega \cos(\omega t + \phi_0), \quad (67)$$

$$\dot{\Omega}_N = 2\bar{\Omega} e \omega \cos(\omega t + \phi_0), \quad (68)$$

with $\omega = (d\phi/dt)(0)$, $\phi_0 = \phi(0)$.

Let us now consider a compact binary inspiral starting at $t = 0$ at initial separation r_0 , with orbital frequency Ω_0 and radial velocity \dot{r}_0 . We take $\dot{r}(t)$ or $\dot{\Omega}(t)$ from a general relativistic inspiral, and fit it with functional forms

$$\dot{r}_{\text{NR}}(t) = S_r(t) + B_r \cos(\omega_r t + \phi_r), \quad (69)$$

$$\dot{\Omega}_{\text{NR}}(t) = S_{\Omega}(t) + B_{\Omega} \cos(\omega_{\Omega} t + \phi_{\Omega}). \quad (70)$$

The subscripts r and Ω indicate whether the fit was performed on \dot{r}_{NR} or $\dot{\Omega}_{\text{NR}}$, and we will use a bullet \bullet in the subscript to represent either r or Ω . The first part of each fit, S_{\bullet} , is a non-oscillatory function that captures the radiation-reaction driven inspiral, whereas the oscillatory piece captures the orbital eccentricity. We neglect spin-induced oscillations. The precise functional form of S_{\bullet} is important, and sometimes it is advisable to include a quadratic term Ct^2 within the argument of the cosine. We comment on these considerations below in Sec. III B

Equation (69) shows that at $t = 0$, orbital eccentricity contributes $\dot{r}_{\text{ecc},0} = B_r \cos \phi_r$ and $\ddot{r}_{\text{ecc},0} = -B_r \omega_r \sin \phi_r$ to the radial velocity and acceleration. Our goal is to now modify the initial data parameters \dot{r}_0 and Ω_0 such that $\dot{r}_{\text{ecc},0}$ and $\ddot{r}_{\text{ecc},0}$ vanish. The radial velocity is a free parameter of the initial data, so $\dot{r}_{0,\text{new}} = \dot{r}_0 + \Delta\dot{r}$, where

$$\Delta\dot{r} = -\dot{r}_{\text{ecc},0} = -B_r \cos \phi_r. \quad (71)$$

To utilize our information about the radial acceleration $\ddot{r}_{\text{ecc},0}$ we recall that for the Newtonian Hamiltonian we have

$$\ddot{r} = \frac{\dot{p}_r}{\mu} = -\frac{1}{\mu} \frac{\partial H_N}{\partial r} = \frac{\mathbf{L}^2}{\mu^2 r^3} - \frac{M}{r^2} = r \Omega^2 - \frac{M}{r^2}. \quad (72)$$

A small change $\Omega_0 \rightarrow \Omega_{0,\text{new}} = \Omega_0 + \Delta\Omega$ therefore changes the radial acceleration by $\Delta\ddot{r} = 2r_0\Omega_0\Delta\Omega$. This change cancels $\ddot{r}_{\text{ecc},0}$ when

$$\Delta\Omega = \frac{B_r \omega_r \sin \phi_r}{2r_0\Omega_0}. \quad (73)$$

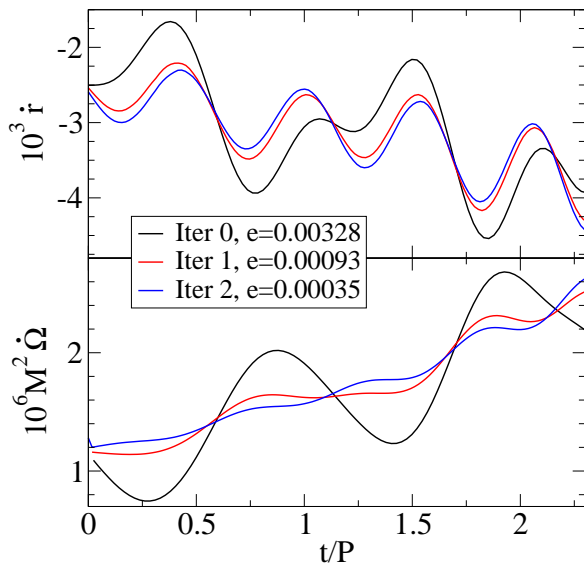


FIG. 3. Eccentricity removal based on $\dot{\Omega}$ applied to a **PN model**. Shown is the initial orbital evolution, and two iterations of eccentricity removal. Parameters of the black-hole binary: mass-ratio $q = 1$, spins of magnitude $\chi_1 = \chi_2 = 0.8$ with initial orientations $(\theta_1 = 0, \phi_1 = 0)$ and $(\theta_2 = \pi/3, \phi_2 = 0)$ with respect to $\hat{\mathbf{L}}_{N0}$ and initial $M\Omega_0 = 0.0315$, that is an initial orbital period $P = 200M$.

Equations (71) and (73) are one version of the updating formulae for the eccentricity removal based on the separation coordinate. A sometimes more effective formula is presented below in Eq. (77) which in earlier numerical work [19, 20, 38] was applied to the *proper separation* between the horizons of the black holes.

A convenient way to derive updating formulae based on $\dot{\Omega}(t)$ begins by noting that the ratio of the amplitudes of oscillations in Eqs. (67) and (68) is $-\bar{r}/(2\bar{\Omega})$. Therefore, we obtain the desired updating formulas by replacing B_r with $-\bar{r}B_\Omega/(2\bar{\Omega})$:

$$\Delta\dot{r} = \frac{r_0 B_\Omega}{2\Omega_0} \cos \phi_\Omega, \quad (74)$$

$$\Delta\Omega = -\frac{B_\Omega \omega_\Omega}{4\Omega_0^2} \sin \phi_r. \quad (75)$$

[A sometimes more effective replacement for Eq. (75) is presented below in Eq. (78).]

In Fig. 3, we present three steps of this eccentricity removal procedure. We use the PN-expanded Hamiltonian with non-spinning terms up to 3PN order [50, 63], and spinning terms up to 2PN order [49, 50]. The radiation-reaction effects are included through 2PN order as in Ref. [50].

We indicate in the legends the value of the eccentricity estimated from the fitted amplitude of the oscillations, once the smooth inspiral has been removed. Note that the initial orbital period is about $200M$. At the 0th step the plots are showing the evolution of the binary system

with initial conditions determined according to the procedure outlined in Ref. [61], leading to the presence of an initial eccentricity. From the plots, we clearly see that we go from a situation dominated by the homogeneous oscillations occurring at the average orbital frequency (step 0) to the situation in which only spin-induced oscillations occurring at twice the average orbital frequency are visible (step 2).

The configuration considered in Fig. 3 is close to merger, where the rapid evolution of the orbit makes it more difficult to apply eccentricity removal. In the next section we discuss how to improve the convergence of the iterative procedure.

B. Practical considerations

Unfortunately, iterative eccentricity removal is sensitive to a variety of effects which are not immediately obvious. Without sufficient care, iterative eccentricity removal converges slowly, or not at all. In this section, we describe important details for the effective and practical application of the eccentricity removal, as well as diagnostics that allow users to evaluate whether the eccentricity removal proceeds optimally.

The fits in Eqs. (69) and (70) are used to compute the values of the oscillating part $B_\bullet \cos(\omega_\bullet t + \phi_\bullet)$ at $t = 0$. Therefore it is crucial that the function S_\bullet that is intended to fit the inspiral portion does *not* fit this oscillatory piece. Initially, we used a polynomial for S_\bullet , but sometimes, especially for shorter fitting intervals, such a polynomial picks up a contribution of the oscillatory piece and results in an unusable fit. Therefore we have constructed more robust fitting functions that cannot capture oscillations. Our current preferred choice is

$$S_\Omega^{(k)} = \sum_{n=0}^{k-1} A_k (T_c - t)^{-11/8-n/4}, \quad (76)$$

with free parameters A_k and T_c . The functional form and the exponents are motivated by PN inspirals, and we keep either $k = 1$ or $k = 2$ terms of this expansion (for $k = 2$, we use the same T_c in both terms).

Another crucial ingredient for a reliable fit is a suitably chosen fitting interval. This interval needs to cover enough oscillations to break degeneracies among the fitting parameters. However, if it becomes too long, the evolution in the inspiral part will be harder to capture with S_\bullet and the quality of the fit will deteriorate.

Finally, the fit is used to compute $\dot{r}_{\text{ecc},0}$ and $\dot{r}_{\text{ecc},0}$, which are quantities at $t = 0$. It is desirable that the fitting interval starts as close to $t = 0$ as possible to minimize extrapolation from the fitting interval to $t = 0$. However, a numerical evolution relaxes in its early stages due a quasi steady-state, and features during this relaxation need to be excluded from the fitting interval.

A good means to ensure a satisfactory fit is to perform several fits, and ensure that the results are consistent.

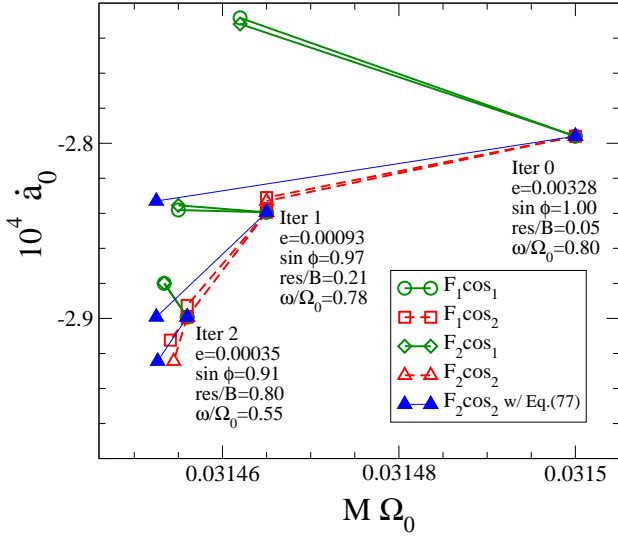


FIG. 4. Visualization of the eccentricity removal performed in Fig. 3 in the Ω_0 - \dot{a}_0 plane. This plot summarizes a large amount of diagnostic information which can be utilized to ensure reliability of the eccentricity removal procedure (see main text). The symbols B , ϕ and ω have a subscript Ω suppressed for clarity.

We perform four distinct fits to $\dot{\Omega}$, where we change the order $k = 1, 2$ of the inspiral component, Eq. (76), and where we change the order of the polynomial within the cosine in Eq. (70) between $l = 1$ as shown in Eq. (70) and $l = 2$ (i.e. adding a quadratic term $C_\bullet t^2$). In addition, we vary the location and length of the fitting interval and check that the updates $\delta\dot{r}$ and $\Delta\Omega$ are unaffected.

Figure 4 demonstrates a useful way to visualize and assess the effectiveness of iterative eccentricity removal. This plot shows the plane of the initial-data parameters Ω_0, \dot{a}_0 , with $\dot{a}_0 = \dot{r}_0/r_0$. The solid symbols correspond to the three PN evolutions shown in Fig. 3. The lines emanating from each of the symbols denote different fits based on this particular evolution. The different fits are denoted $F_k \cos_l$, where $k = 1, 2$ denotes the fitting order in S_\bullet and l denotes the order of the polynomial inside the cosine. Each of these lines ends at the predicted improved parameters $\Omega_{0,\text{new}}, \dot{a}_{0,\text{new}}$. Clustering of these lines, and convergence of the symbols indicates that eccentricity removal is proceeding well. As can be seen by comparing the solid dark green and dashed red curves, the order k of the fitting function for the smooth part S_Ω has almost no impact on the updated parameters $\Omega_{0,\text{new}}, \dot{a}_{0,\text{new}}$ in this case. However, using a quadratic polynomial inside the cosine ($l = 2$) significantly improves the quality of the Ω_0 -update.

Figure 4 can also be used to assess the potential quality for different updating formulae. While we have kept the orbital frequency Ω_0 separate from the eccentricity oscillation frequency ω_Ω , for Newtonian orbits both frequencies agree. Therefore, our Newtonian motivation does not provide a means to choose whether to include extra

powers of Ω_0/ω_Ω . Specifically, we could replace Eqs. (73) and (75) by either

$$\Delta\Omega = -\frac{B_r}{2r_0} \sin\phi_r, \quad (77)$$

or

$$\Delta\Omega = -\frac{B_\Omega}{4\Omega_0} \sin\phi_\Omega, \quad (78)$$

for updates based on $\dot{r}(t)$ and $\dot{\Omega}(t)$, respectively. The predictions of the updating formula Eq. (77) are shown in Fig. 4 as filled blue triangles. It is obvious that Eq. (77) predicts an updated Ω_0 significantly closer to the final best value for Ω_0 , even when applied to Iter 0. Therefore, to summarize the discussion in the preceding paragraphs, for most effective eccentricity removal we recommend the fit of the form $F_2 \cos_2$ combined with Eq. (77).

Finally, we discuss several diagnostics that can help to assess the quality of eccentricity removal, and which are included next to each symbol in Fig. 4. The first diagnostic is the estimated eccentricity e , which should be monotonically decaying. The second diagnostic is $\sin\phi_\Omega$. As can be seen from Eqs. (74) and (75), the angle ϕ_Ω parametrizes the relative importance of the Ω_0 and \dot{a}_0 updates. For $\sin\phi_\Omega \approx 1$, the whole weight is carried by the Ω_0 update. This is the case here, and indicates that the starting value for \dot{a}_0 was already very good, and that the apparent inconsistent predictions for $\dot{a}_{0,\text{new}}$ will not have an adverse impact on the eccentricity fitting procedure (note that all fits predict consistent values for $\Omega_{0,\text{new}}$). The third diagnostic is the ratio of the root-mean-square residual of the fit, res , to the amplitude of the oscillatory part, B_Ω . When $\text{res}/B \ll 1$, then $\dot{\Omega}$ has indeed the assumed form Eq. (70), a prerequisite for eccentricity removal. When $\text{res}/B \sim 1$, we can no longer isolate the oscillatory piece, and eccentricity removal ceases to be effective. The final diagnostic is the ratio of frequencies of radial oscillations ω_Ω to orbital frequency Ω_0 . For a good fit, ω_Ω/Ω_0 should be somewhat less than unity, where the deviation from unity is caused by periastron advance. For moderately small eccentricities, this ratio should furthermore be independent of the precise value of eccentricity. This is indeed the case for “Iter 0” and “Iter 1”, but “Iter 2” results in a questionably small ratio, which furthermore differs from the values for iterations 0 and 1. Again, an indication that we cannot further proceed with eccentricity removal.

IV. APPLICATION TO FULLY NUMERICAL BINARY BLACK-HOLE SIMULATIONS

We now apply the method outlined in Sec. III to reduce the initial eccentricity of single-spin and double-spin precessing binary black-hole simulations. We compare the periodicity in the oscillations of the orbital frequency and the proper horizon separation to the PN predictions described in Sec. II and also to the periastron-advance results of Ref. [42]. Finally, for one binary configuration, we

also extract the $l = 2, m = 2$ mode of the gravitational waveform and investigate the presence of spin-induced oscillations in its phase and frequency.

A. Numerical methods

Binary black hole initial data is constructed using the conformal thin sandwich formalism [64, 65] and quasi-equilibrium boundary conditions [28, 66, 67], incorporating radial velocity as described in Ref. [34]. The resulting set of five nonlinear coupled elliptic equations is solved with multi-domain pseudo-spectral techniques described in Ref. [68]. As in earlier work, we choose conformal flatness and maximal slicing. To obtain desired masses and spins, we utilize a root-finding procedure to adjust freely specifiable parameters in the initial data [40].

Thus, a binary black-hole initial data set is determined by the mass-ratio, the spins of both black holes, and coordinate separation d between the coordinate centers of the black holes, orbital frequency Ω_0 , and radial velocity $\dot{r}_0 = \dot{a}_0 d$, where \dot{a}_0 is the dimensionless expansion factor. For fixed d , eccentricity removal consists of finding values for Ω_0 and \dot{a}_0 that result in sufficiently small eccentricity.

The constructed initial data are evolved with the Spectral Einstein Code SpEC [69]. This code evolves a first-order representation [70] of the generalized harmonic system [71–73] and includes terms that damp away small constraint violations [70, 73, 74]. The computational domain extends from excision boundaries located just inside each apparent horizon to some large radius. No boundary conditions are needed or imposed at the excision boundaries, because all characteristic fields of the system are outgoing (into the black hole) there. The boundary conditions on the outer boundary [70, 75, 76] are designed to prevent the influx of unphysical constraint violations [77–83] and undesired incoming gravitational radiation [84, 85], while allowing the outgoing gravitational radiation to pass freely through the boundary. Interdomain boundary conditions are enforced with a penalty method [86, 87].

B. Eccentricity removal based on orbital frequency: single-spin binary black hole

In this section we re-visit eccentricity removal for the configuration considered in the introduction and Fig. 1. The binary has a mass-ratio of $m_1/m_2 = 1.5$, and only the larger black hole carries spin, namely $\chi_1 = 0.5$ with initial spin direction in the orbital plane pointing exactly away from the smaller black hole. Note that spins in the orbital plane maximize spin-induced oscillations [see, e.g., Eqs. (44) and (45)]. The initial coordinate separation between the holes is $d = 16M$, orbital frequency $M\Omega_0 = 0.0142$, and $\dot{a}_0 = -5 \times 10^{-5}$. These parameters were determined from the so-called TaylorT3 PN approximant for non-spinning binaries [16].

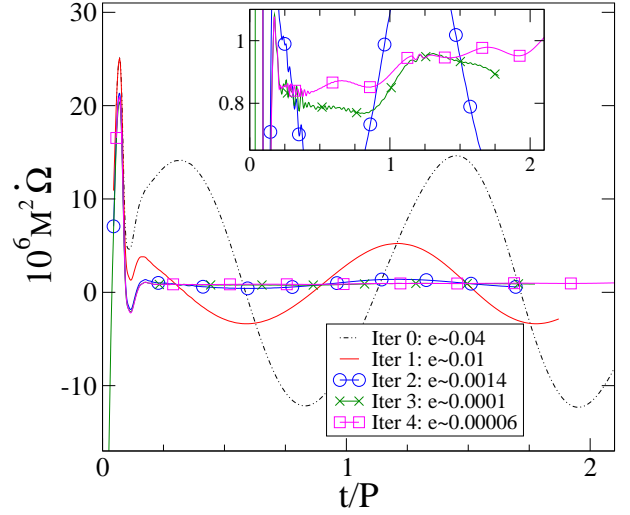


FIG. 5. **Eccentricity removal based on time derivative of the orbital frequency $d\Omega/dt$** , applied to a single-spin *precessing* binary black hole with the same initial parameters as in Fig. 1. Shown is $\dot{\Omega}$ vs. time in units of initial orbital period $P = 442M$ for the initial run (based on PN parameters) and four eccentricity-removal iterations. The amplitude of spin-induced oscillations is several orders of magnitude smaller than in Fig. 1, and becomes only visible in Iter 4.

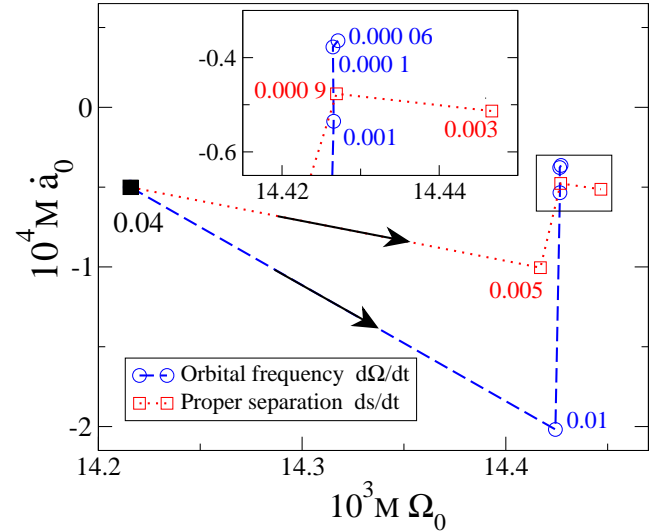


FIG. 6. **Convergence of the eccentricity-removal procedures in the (Ω_0, \dot{a}_0) plane.** Blue circles: eccentricity removal sequence of Fig. 5. Red squares: eccentricity removal sequence shown in Fig. 1. The number next to each symbol gives the eccentricity of the respective evolution. The inset shows an enlargement of the boxed area. The eccentricity-removal procedure based on the orbital frequency keeps converging until the fourth iteration, while the one based on the proper separation fails to converge any further beyond the second iteration.

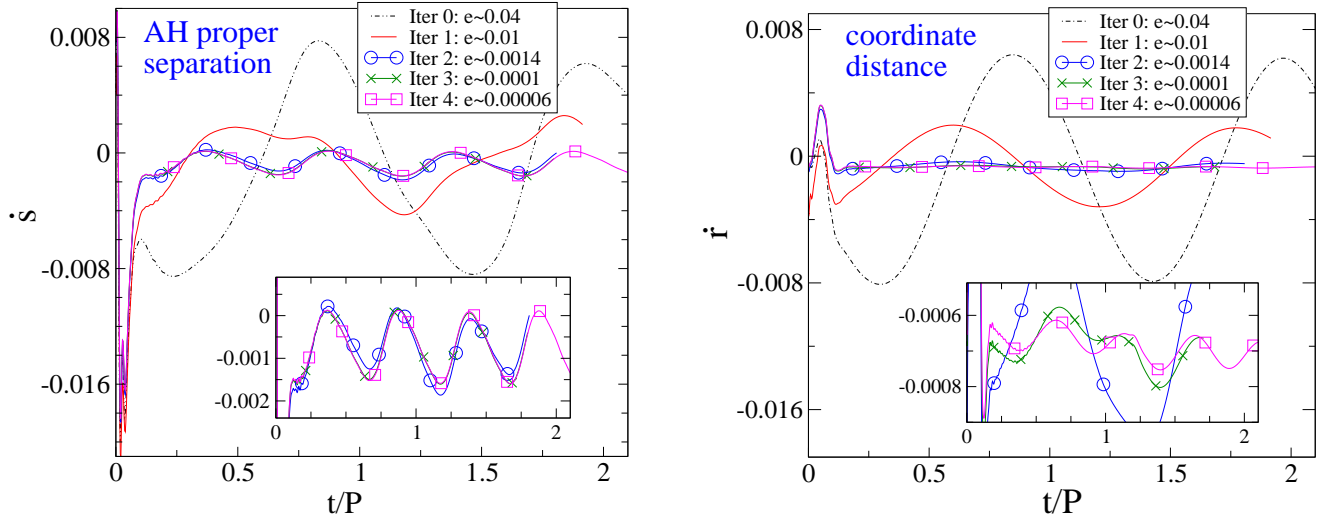


FIG. 7. **Radial velocity** between the black holes for the same series of evolutions shown in Fig. 5. **Left:** Derivative of proper separation between the apparent horizons \dot{s} . **Right:** Derivative of coordinate distance between centers of the apparent horizons \dot{r} . The time-axis is given in units of the initial orbital period $P = 442M$. Proper separation \dot{s} exhibits large spin-induced oscillations, whereas \dot{r} shows spin-induced oscillations of similarly small amplitude as in Fig. 5. Note that the inset in the right panel is ten times more magnified than in the left panel.

Orbital frequency, both in the initial data and in the subsequent evolution, is defined by the coordinate motion of the center of the apparent horizons. Let $\mathbf{c}_i(t)$ be the coordinates of the center of each black hole, and define their relative separation $\mathbf{r}(t) = \mathbf{c}_1(t) - \mathbf{c}_2(t)$. The instantaneous orbital frequency is then computed as

$$\Omega = \frac{\mathbf{r} \times \dot{\mathbf{r}}}{r^2}, \quad (79)$$

and Ω is defined as the magnitude of Ω . All these calculations are performed using standard Euclidean vector calculus.

We start the first run using PN initial conditions for the orbital frequency and radial velocity and evolve the binary black hole for about two orbits. From the orbital frequency we measure an eccentricity $e \sim 0.04$, and Eqs. (74) and (75) give improved values for Ω_0 and \dot{a}_0 . Evolution of the initial data computed from these improved values is labeled “Iter 1” in Fig. 5, and reduces the eccentricity to about 0.01. The same procedure is then repeated three more times. For Iter 0 to Iter 2, we exclude $t \lesssim 100M$ from the fit. For Iter 3 the variations in $\dot{\Omega}$ are so small that numerical noise is dominant for about half an orbital period, and we exclude $t \lesssim 250M$ from the fit. The final eccentricity in the orbital frequency is $e \sim 6 \times 10^{-5}$.

In Fig. 6, we show how the initial orbital frequency Ω_0 and the radial expansion factor \dot{a}_0 converge to the final values (minimal eccentricity). The blue circles indicate the successive iterations for the successful eccentricity removal based on $\dot{\Omega}$ (see Fig. 5). Note that the parameters (Ω_0, \dot{a}_0) converge well for all iterations. In contrast, the red squares denote the unsuccessful eccentricity removal based on proper separation \dot{s} (see Fig. 1). Starting with

the third iteration, the updated values of the orbital frequency and expansion radial coefficient move away from the line of minimum eccentricity, with an increase of eccentricity from 0.001 to 0.003. All eccentricity estimates shown in this figure are computed from $\dot{\Omega}$, even when eccentricity removal is based on \dot{s} . This allows us to measure eccentricities $e < 0.01$, which would not be possible from \dot{s} , because the latter is dominated by large spin-induced oscillations.

The absence of spin-induced oscillations in Fig. 5 is striking, especially when compared to Fig. 1. Spin-induced oscillations are visible in Fig. 5 only at $e < 10^{-4}$. For the runs with larger eccentricity (Iter 0–3), eccentricity-induced oscillations dominate with a period somewhat larger than P (somewhat larger because of periastron-advance [42]).

We shall now investigate spin-induced oscillations in the numerical-relativity simulations in more detail. First, by comparing the time-derivatives of orbital frequency $\dot{\Omega}$, proper separation between horizons \dot{s} , and coordinate separation between centers of apparent horizons \dot{r} . Subsequently, by comparing their amplitude and frequency with PN predictions from Sec. II.

Figure 7 shows time-derivatives of proper separation \dot{s} and coordinate separation \dot{r} for the evolutions shown in Fig. 5. Spin-induced oscillations are already noticeable in \dot{s} for Iter 1 with $e = 0.01$. These oscillations dominate for Iter 2–4, i.e. $e \leq 0.0014$. In contrast, the coordinate distance \dot{r} is less susceptible to spin-induced oscillations. In the right plot of Fig. 7, spin-induced oscillations become apparent only for eccentricities of $\sim 10^{-4}$ or smaller. The spin-induced oscillations in \dot{r} are smaller by a factor of almost 20 than those in \dot{s} .

When comparing Iter 3 and Iter 4 between Fig. 5 and

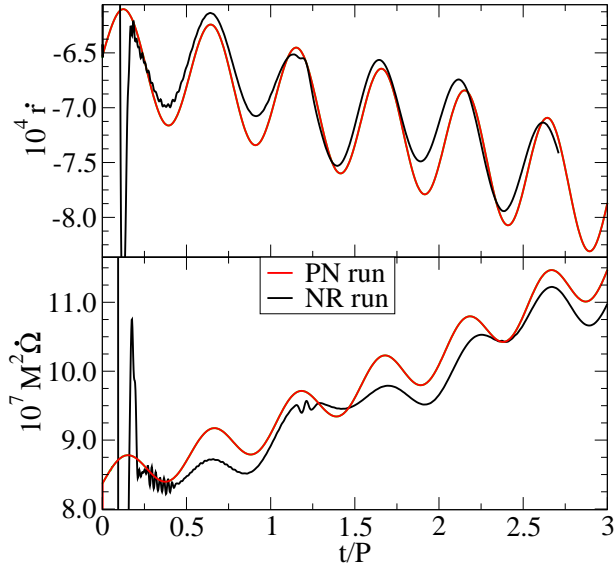


FIG. 8. Spin-induced oscillations of the lowest-eccentricity numerical simulation (Iter 4 of Fig. 5) in comparison with the PN calculations of Sec. II C.

the right panel of Fig. 7, one notices that $\dot{\Omega}$ shows slightly less pronounced spin-induced oscillations. That is consistent with the PN calculations, where Eq. (64) predicted that spin-induced oscillations in $\dot{\Omega}$ should be suppressed by a factor of 2 relative to those in \dot{r} . When comparing Iter 4 between Fig. 5 and the right plot of Fig. 7, we find that the spin-induced oscillations in $\dot{\Omega}$ and \dot{r} are *in phase*. This is again consistent with the PN prediction, where the last terms of Eqs. (46) and (47) have the same sign. The phase of spin-induced oscillations in $\dot{\Omega}$ and \dot{r} differs from the effect of orbital eccentricity: for an eccentric orbit, the orbital frequency is maximal when the separation is minimal, and therefore $\dot{\Omega}$ and \dot{r} are out of phase (see Iter 0 and Iter 1 of Figs. 5 and 7).

We have shown in Sec. II C that the PN Hamiltonian predicts spin-induced oscillations: Equations (46)–(49) contain an oscillatory component at twice the orbital frequency with amplitudes

$$A_{\delta\dot{r}} = \frac{\bar{\Omega} \mathbf{S}_{0\perp}^2}{2M^2 \bar{r}}, \quad (80)$$

$$A_{\delta\dot{\Omega}} = \frac{\bar{\Omega}^2 \mathbf{S}_{0\perp}^2}{2M^2 \bar{r}^2}. \quad (81)$$

Figure 8 shows numerical data for the lowest-eccentricity numerical simulation (Iter 4 from Fig. 5). These numerical data are compared with the prediction of the PN equations. The PN calculation reproduces very accurately the amplitude of spin-induced oscillations in the numerical-relativity simulation for $\dot{\Omega}$ and \dot{r} . By contrast, the spin-induced oscillations in \dot{s} are larger by a factor ~ 20 than those in \dot{r} . This can be due to deformations of the apparent horizons due to spin effects. Finally, we notice that a small amplitude oscillation of the numerical data on the orbital time-scale is also visible, correspond-

ing to the small, but non-zero eccentricity $e = 6 \times 10^{-5}$ of the numerical simulation.

C. Oscillations in the (2,2) mode of the gravitational wave

In Sec. IV B we found spin-induced oscillations in the coordinate distance of the black holes and the orbital frequency, consistent with PN predictions. We now investigate the gravitational radiation emitted by this binary. Specifically, we extract the $l = 2, m = 2$ mode of the gravitational waveform in the inertial frame where the binaries are *initially* placed along the x -axis and the initial angular momentum is parallel to the z -axis. We compute phase and frequency for the waveforms extracted at extraction radii $R = 130M$ and $R = 220M$.

Spin-induced oscillations represent a physical effect independent of orbital eccentricity. Nevertheless, the concept of eccentricity estimators [42] will be very useful when discussing spin-induced oscillations, because it removes overall secular trends (especially in the gravitational-wave phase), and because it makes it easy to relate the amplitude of oscillations to an “equivalent eccentricity.” As Ref. [42], we define $e_{\phi_{\text{GW}}}(t)$

$$e_{\phi_{\text{GW}}}(t) = \frac{\phi_{\text{NR}}(t) - \phi_{\text{fit}}(t)}{4}, \quad (82)$$

where $\phi_{\text{NR}}(t)$ is the gravitational-wave phase of the (2,2) mode and $\phi_{\text{fit}}(t)$ is the quasi-circular polynomial fit of the gravitational-wave phase [see Ref. [42] for more details]. Similarly, using the gravitational-wave frequency of the (2,2) mode and its quasi-circular polynomial fit as in Ref. [42], we define the eccentricity estimator $e_{\omega_{\text{GW}}}(t)$

$$e_{\omega_{\text{GW}}}(t) = \frac{\omega_{\text{NR}}(t) - \omega_{\text{fit}}(t)}{2\omega_{\text{fit}}(t)}. \quad (83)$$

In Fig. 9, we plot the eccentricity estimators $e_{\phi_{\text{GW}}}(t)$ (upper panel) and $e_{\omega_{\text{GW}}}(t)$ (lower panel) for the two extraction radii $R = 130M$ and $R = 220M$ versus the retarded time $t - R^*$, where R^* is the tortoise-coordinate radius defined as

$$R^* \equiv R + 2M \ln \left(\frac{R}{2M} - 1 \right), \quad (84)$$

where $M = 1$ is the total mass of the initial data. Quite interestingly, the plots show oscillations happening at twice the orbital frequency. The magnitude of the oscillations in $e_{\phi_{\text{GW}}}(t)$ or $e_{\omega_{\text{GW}}}(t)$ is $\sim 10^{-3}$, although the eccentricity in the orbital frequency has been reduced to $\sim 6 \times 10^{-5}$ (see Fig. 5). We note that the amplitude of the oscillations at twice the orbital frequency does not depend on the extraction radius, suggesting that they are gauge invariant.

We also compare these numerical result with what is predicted by the PN model. For the orbital evolution we use the model Hamiltonian (6), where SO and SS

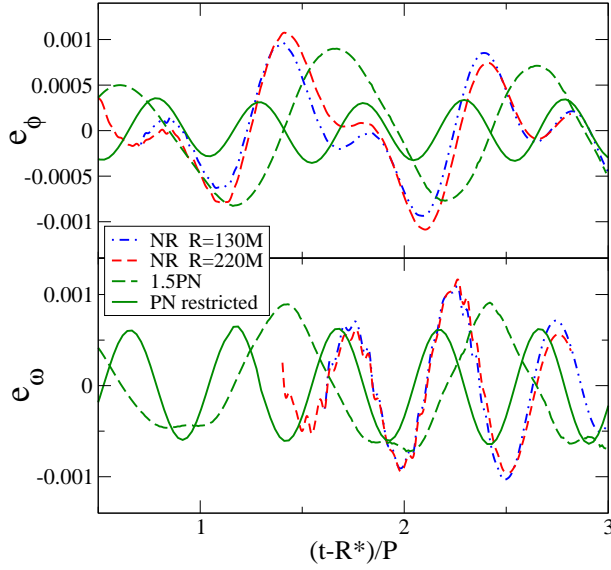


FIG. 9. **Eccentricity estimator for the gravitational-wave phase and frequency** for the final eccentricity-removal iteration of Fig. 5. The upper panel shows the gravitational-wave-phase eccentricity estimator for two extraction radii versus the retarded time, the lower panel the eccentricity estimator computed from the gravitational wave frequency. In both panels we clearly see oscillations at twice the orbital frequency. We also show the PN result for the restricted waveform.

interactions are included through 2PN order, nonspinning effects through 3PN order, and radiation-reaction effects through 2PN order. As to the analytical model, we employ the waveform derived in Ref. [88], where the precession of the orbital plane and the spins of the black holes are taken into account through 1.5PN order. In particular, we compute the estimators $e_{\phi_{\text{GW}}}$ and $e_{\omega_{\text{GW}}}$ using Eqs. (4.15), (4.16a) in Ref. [88] for the h_{22} mode with the amplitude computed at lowest order in v/c (restricted waveform)⁴. This means that the precession of the orbital plane is considered only in the gravitational-wave phase, but not in the amplitude.

Before computing the PN eccentricity estimators, we perform an alignment between the phase of the PN h_{22} and the phase of the numerical-relativity Ψ_4 . To do that, we follow the procedure outlined in Sec. IIIA of Ref. [9]. This alignment is obtained over a time window of $1000M$ (in the range $500M < t < 1500M$), and it amounts to a time-shift and a global offset in the PN phase. The result is shown as solid black curves in Fig. 9. We see a qualitative agreement between numerical-relativity results and the restricted PN model for the oscillations at

⁴ Since the numerical-relativity (2,2) mode is computed using as z -axis the direction perpendicular to the orbital plane, we apply the Wigner rotation to the restricted h_{22} of Ref. [88] and keep only the lowest-order term in v/c .

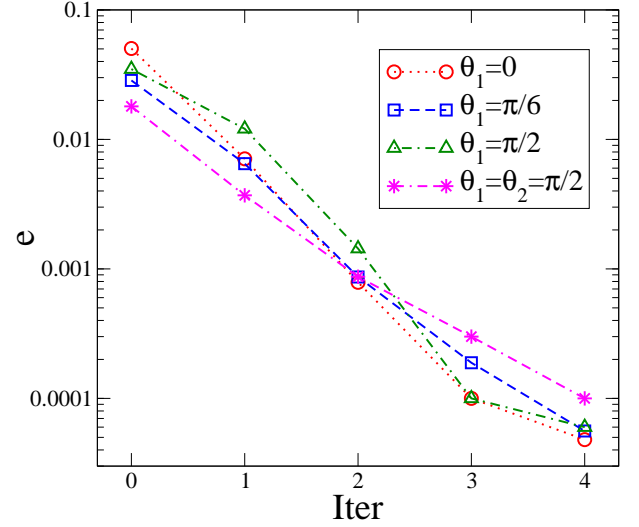


FIG. 10. **Eccentricity removal for different spin-configurations.** We illustrate of how the eccentricity is reduced to very low values when the iterations are applied to the orbital frequency. Shown are three configurations with $S_1/M_1^2 = 0.5, S_2 = 0$ and different spin directions θ_1 , and one configuration with $S_1/M_1^2 = S_2/M_2^2 = 0.5$, with initially two orthogonal spins both tangent to the orbital plane. For all cases, the mass-ratio is $m_1/m_2 = 1.5$. The run shown in green triangles was discussed in detail in Figs. 5 to 9.

twice the orbital frequency in $e_{\omega_{\text{GW}}}$ and $e_{\phi_{\text{GW}}}$. However, the numerical-relativity $e_{\phi_{\text{GW}}}$ also shows oscillations at the orbital frequency which are absent in the restricted PN waveform. We find that oscillations at the orbital frequency can be generated in the PN model of Ref. [88] if we included higher order PN corrections in the amplitude of the (2,2) mode [see Eq. (4.16a) in Ref. [88]]. Such oscillations cannot be iterated away by our procedure, even in principle, since the removal algorithm concerns the orbital dynamics and they rather appear as a physical effect of the waveform. The upper panel of Fig. 9 shows comparatively large oscillations at period $\sim P$; because the PN model predicts modes at this frequency, these oscillations cannot be used to compute orbital eccentricity. A further analysis of the inclusion of higher-order PN corrections is warranted. We prefer to postpone such an analysis to be able to test against a larger sample of numerical-relativity waveforms.

D. Eccentricity-removal for generic binary black holes

In the previous sections we studied our new eccentricity-removal procedure in detail for one test-case: a binary with only one non-zero spin, and with mass-ratio $m_1/m_2 = 1.5$. We now test the procedure for other binary configurations with the same mass ratio. We consider two further configurations where only the large black hole carries spin, parametrized by the angle

θ_1 between the orbital angular momentum and the spin axis of the first black hole. In the previous sections, we considered $\theta_1 = \pi/2$, and now we extend to $\theta_1 = 0, \pi/6$, and $\phi_1 = 0$. The first of these new cases is non-precessing and verifies that eccentricity removal based on $\dot{\Omega}$ works effectively for non-precessing systems. We also consider a binary where both black holes carry spin, with initial spin-direction in the orbital plane ($\theta_1 = \theta_2 = \pi/2$), \mathbf{S}_1 parallel to the initial separation vector between the black holes, and \mathbf{S}_2 normal to the separation vector. (All spinning black holes have dimensionless spin-magnitude of 0.5.) Figure 10 demonstrates the effectiveness of the eccentricity removal procedure based on $\dot{\Omega}$ and Eqs. (74) and (75). In all cases, the eccentricity is reduced to less than 10^{-4} in four iterations.

The number of required eccentricity removal iterations depends on the quality of the guess for Ω_0 and \dot{a}_0 for the first iteration. Once eccentricity removal has been performed for several different configurations, we expect to be able to interpolate between configurations, to improve the initial guess substantially.

V. CONCLUSIONS

The removal of the initial spurious orbital eccentricity in binary black-hole simulations is quite challenging, and it becomes more complicated in the presence of spins. As predicted by PN theory, and worked out in Sec. II, spin-spin interactions (notably $S_1 S_1$, $S_2 S_2$ and $S_1 S_2$ terms) and precession induce oscillations in the binary radial separation and orbital frequency. These *spin-induced oscillations* are also present in the gravitational radiation emitted by the binary, and their frequency is close to twice the average orbital frequency. In Sec. IV we confirm the presence of spin-induced oscillations in fully numerical simulations of black hole binaries. The agreement between the numerical simulations and PN calculations is as good as can be expected given the low order of the PN calculations, and the differing coordinate gauges.

Spin-induced oscillations can be distinguished from oscillations caused by orbital eccentricity by their characteristic frequencies. Moreover, the amplitude of spin-induced oscillations is quite small, so that it becomes visible only at small eccentricities, as can be seen from Eq. (51): At separations relevant for numerical simulations, spin-induced oscillations dominate orbital eccentricity only for $e \lesssim 0.001$, even for maximal spins in the least favorable orientation (parallel spins in the orbital plane). The amplitude of spin-induced oscillations is proportional to $S_{0,\perp}^2$, so that for spin $S/M^2 \sim 0.5$ as considered here, spin-induced oscillations become visible at orbital eccentricity $e \sim 10^{-4}$.

Spin-induced oscillations affect the orbital frequency derivative $\dot{\Omega}$ less than the radial velocity \dot{r} . Therefore, we develop in Sec. III a new eccentricity-removal procedure based on the derivative of the orbital frequency, and apply it to PN inspirals. Subsequently, we success-

fully apply the eccentricity removal procedure to fully numerical binary black hole evolutions to achieve eccentricities smaller than 10^{-4} . At this residual eccentricity, spin-induced oscillations begin to dominate over orbital eccentricity oscillations, as expected from our PN calculations. In Sec. IV D, we tested the new eccentricity-removal procedure on fully numerical binary black hole simulations for several different spin configurations.

The computational cost for eccentricity reduction depends on the number of eccentricity removal iterations. Great care is necessary when performing the fitting, in order to achieve a large reduction in eccentricity per iteration. Section III B gives guidance to improve these fits. With a good initial guess of Ω_0, \dot{a}_0 for the 0-th iteration, one can start eccentricity removal from an already small initial eccentricity. As the number of data-points increases, we expect to be able to compute a better initial guess by interpolating between already computed low-eccentricity binary black-hole configurations.

Perhaps surprising, our present study indicates that eccentricity removal should *not* be based on the proper separation between the apparent horizons. These new findings supersede the practice of earlier papers [19, 20, 38] to base eccentricity removal on proper separation rather than coordinate separation to take advantage of reduced numerical noise. As apparent in Figs. 7 and 8, spin-induced oscillations in \dot{s} are about 15 times larger than in \dot{r} . Therefore, eccentricity-removal based on \dot{s} will fail at ~ 15 times larger eccentricity than using \dot{r} , and at ~ 30 times larger eccentricity than for $\dot{\Omega}$. A likely cause for the unsatisfactory behavior of \dot{s} lies in the deformation of the apparent horizons due to spin. For spins with a component in the orbital plane, the “bulge” of the apparent horizon rotates through the line connecting the two black holes as the black holes orbit each other. Earlier work [19, 20, 38] considered spins aligned with the orbital angular momentum, where this effect is absent; in those cases use of \dot{s} was in order — but for precessing binaries, use of \dot{s} is not advisable.

Even when the orbital frequency indicates $e < 10^{-4}$ for a fully numerical binary black-hole simulation, the extracted (2,2) mode of the gravitational radiation still shows oscillations at the orbital frequency in the wave phase with amplitude $\sim 10^{-3}$. While future work is necessary for a detailed understanding, the PN model predicts oscillations in the GW at the orbital frequency, and therefore, one cannot use the gravitational waveforms to estimate orbital eccentricity for precessing binaries. The wave phase and frequency of the NR simulation also shows oscillations at twice the orbital frequency with amplitude $\sim 3 \times 10^{-4}$ which are qualitatively reproduced by the restricted PN model of Ref. [88]. We postpone the study of the details of these features in the gravitational waveform to future work. Quite interestingly, it proves, for this particular binary configuration in which only one hole spins, that those spin-induced oscillations are a direct consequence of monopole-quadrupole interactions [44, 45, 49, 89, 90].

All fully relativistic simulations presented here were performed using generalized harmonic coordinates. It would be very interesting to perform a similar study within the moving-puncture BSSN approach to investigate whether our conclusions are applicable in other gauges.

ACKNOWLEDGMENTS

We thank Guillaume Faye, Geoffrey Lovelace, Evan Ochsner and Yi Pan for useful interactions. The presented binary black hole evolutions were performed using the Spectral Einstein Code SpEC [69]. A.B.

and A.T. acknowledge support from NSF Grant PHY-0903631. A.B. also acknowledges support from NASA grant NNX09AI81G. A.T. also acknowledges support from the Maryland Center for Fundamental Physics. L.K. is supported by NSF Grants No. PHY-0969111 and No. PHY-1005426 at Cornell; and by NASA Grant No. NNX09AF96G at Cornell. H.P. gratefully acknowledges support from the NSERC of Canada, from Canada Research Chairs Program, and from the Canadian Institute for Advanced Research. Computations were performed on the GPC supercomputer at the SciNet HPC Consortium. SciNet is funded by: the Canada Foundation for Innovation under the auspices of Compute Canada; the Government of Ontario; Ontario Research Fund - Research Excellence; and the University of Toronto.

-
- [1] M. Hannam, *Class. Quant. Grav.* **26**, 114001 (2009).
 - [2] I. Hinder, *Class. Quant. Grav.* **27**, 114004 (2010).
 - [3] J. M. Centrella, J. G. Baker, B. J. Kelly, and J. R. van Meter, *Rev. Mod. Phys.* **82**, 3069 (2010).
 - [4] A. Buonanno, Y. Pan, J. G. Baker, J. Centrella, B. J. Kelly, S. T. McWilliams, and J. R. van Meter, *Phys. Rev. D* **76**, 104049 (2007).
 - [5] P. Ajith, S. Babak, Y. Chen, M. Hewitson, B. Krishnan, A. M. Sintes, J. T. Whelan, B. Brügmann, P. Diener, N. Dorband, J. Gonzalez, M. Hannam, S. Husa, D. Pollney, L. Rezzolla, L. Santamaría, U. Sperhake, and J. Thornburg, *Phys. Rev. D* **77**, 104017 (2008).
 - [6] T. Damour and A. Nagar, *Phys. Rev. D* **79**, 081503 (2009).
 - [7] A. Buonanno, Y. Pan, H. P. Pfeiffer, M. A. Scheel, L. T. Buchman, and L. E. Kidder, *Phys. Rev. D* **79**, 124028 (2009).
 - [8] P. Ajith, M. Hannam, S. Husa, Y. Chen, B. Brügmann, N. Dorband, D. Mueller, F. Ohme, D. Pollney, C. Reisswig, L. Santamaría, and J. Seiler(2009), [arXiv:0909.2867 \[gr-qc\]](#).
 - [9] Y. Pan, A. Buonanno, L. Buchman, T. Chu, L. Kidder, H. Pfeiffer, and M. Scheel, *Phys. Rev. D* **81**, 084041 (2010).
 - [10] B. Aylott *et al.*, *Classical and Quantum Gravity* **26**, 165008 (2009).
 - [11] P. C. Peters and J. Mathews, *Phys. Rev.* **131**, 435 (Jul 1963).
 - [12] P. C. Peters, *Phys. Rev.* **136**, B1224 (Nov 1964).
 - [13] K. Postnov and L. Yungelson, *Living Rev. Rel.* **9**, 6 (2005), [arXiv:astro-ph/0701059](#).
 - [14] M. Miller and D. Hamilton, *Astrophys. J.* **576**, 894 (2002).
 - [15] L. Wen, *Astrophys. J.* **598**, 419 (2003).
 - [16] L. Blanchet, *Living Rev. Rel.* **9** (2006).
 - [17] H. P. Pfeiffer, G. B. Cook, and S. A. Teukolsky, *Phys. Rev. D* **66**, 024047 (2002).
 - [18] S. Dain, C. O. Lousto, and Y. Zlochower, *Phys. Rev. D* **78**, 024039 (2008), [arXiv:0803.0351v2 \[gr-qc\]](#).
 - [19] G. Lovelace, R. Owen, H. P. Pfeiffer, and T. Chu, *Phys. Rev. D* **78**, 084017 (2008).
 - [20] T. Chu, H. P. Pfeiffer, and M. A. Scheel, *Phys. Rev. D* **80**, 124051 (2009).
 - [21] G. B. Cook, *Phys. Rev. D* **50**, 5025 (1994).
 - [22] T. W. Baumgarte, *Phys. Rev. D* **62**, 024018 (2000).
 - [23] H. P. Pfeiffer, S. A. Teukolsky, and G. B. Cook, *Phys. Rev. D* **62**, 104018/1 (2000).
 - [24] E.ourgoulhon, P. Grandclément, and S. Bonazzola, *Phys. Rev. D* **65**, 044020 (2002).
 - [25] P. Grandclément, E.ourgoulhon, and S. Bonazzola, *Phys. Rev. D* **65**, 044021 (2002).
 - [26] W. Tichy, B. Brügmann, and P. Laguna, *Phys. Rev. D* **68**, 064008 (2003).
 - [27] W. Tichy and B. Brügmann, *Phys. Rev. D* **69**, 024006 (2004), [gr-qc/0307027](#).
 - [28] M. Caudill, G. B. Cook, J. D. Grigsby, and H. P. Pfeiffer, *Phys. Rev. D* **74**, 064011 (2006).
 - [29] J. D. Grigsby and G. B. Cook, *Phys. Rev. D* **77**, 044011 (2008), [arXiv:0706.4286 \[gr-qc\]](#).
 - [30] F. Pretorius, *Phys. Rev. Lett.* **95**, 121101 (2005).
 - [31] J. G. Baker, J. Centrella, D.-I. Choi, M. Koppitz, and J. van Meter, *Phys. Rev. Lett.* **96**, 111102 (2006).
 - [32] M. Campanelli, C. O. Lousto, P. Marronetti, and Y. Zlochower, *Phys. Rev. Lett.* **96**, 111101 (2006).
 - [33] A. Buonanno, G. B. Cook, and F. Pretorius, *Phys. Rev. D* **75**, 124018 (2007).
 - [34] H. P. Pfeiffer, D. A. Brown, L. E. Kidder, L. Lindblom, G. Lovelace, and M. A. Scheel, *Class. Quantum Grav.* **24**, S59 (2007).
 - [35] J. G. Baker, J. R. van Meter, S. T. McWilliams, J. Centrella, and B. J. Kelly, *Phys. Rev. Lett.* **99**, 181101 (2007).
 - [36] S. Husa, M. Hannam, J. A. González, U. Sperhake, and B. Brügmann, *Phys. Rev. D* **77**, 044037 (2008), [arXiv:0706.0904 \[gr-qc\]](#).
 - [37] B. Walthier, B. Brügmann, and D. Mueller, *Phys. Rev. D* **79**, 124040 (2009), [arXiv:0901.0993 \[gr-qc\]](#).
 - [38] M. Boyle, D. A. Brown, L. E. Kidder, A. H. Mroué, H. P. Pfeiffer, M. A. Scheel, G. B. Cook, and S. A. Teukolsky, *Phys. Rev. D* **76**, 124038 (2007).
 - [39] W. Tichy and P. Marronetti(2010), [arXiv:1010.2936 \[gr-qc\]](#).
 - [40] L. T. Buchman, H. P. Pfeiffer, and M. A. Scheel, “Simulations of non-equal mass black hole binaries,” In preparation.
 - [41] G. Lovelace, M. A. Scheel, and B. Szilagyi(2010),

- arXiv:1010.2777 [gr-qc].
- [42] A. H. Mroue, H. P. Pfeiffer, L. E. Kidder, and S. A. Teukolsky(2010), arXiv:1004.4697 [gr-qc].
 - [43] L. E. Kidder, Phys. Rev. **D52**, 821 (1995).
 - [44] E. Poisson, Phys. Rev. **D57**, 5287 (1998).
 - [45] E. Racine, A. Buonanno, and L. E. Kidder, Phys. Rev. D **80**, 044010 (2009).
 - [46] M. Maggiore, *Gravitational Waves - Volume 1*, 1st ed. (Oxford University Press, New York, NY, 2008).
 - [47] T. Damour and G. Schäfer, Nuovo Cimento Soc. Ital. Fis. **101 B**, 127 (1988).
 - [48] B. M. Barker and R. F. O'Connell, Phys. Rev. **D12**, 329 (1975).
 - [49] T. Damour, Phys. Rev. D **64**, 124013 (2001).
 - [50] A. Buonanno, Y. Chen, and T. Damour, Phys. Rev. D **74**, 104005 (2006).
 - [51] T. Damour, P. Jaranowski, and G. Schaefer, Phys. Rev. **D77**, 064032 (2008), arXiv:0711.1048 [gr-qc].
 - [52] R. A. Porto, Class. Quant. Grav. **27**, 205001 (2010), arXiv:1005.5730 [gr-qc].
 - [53] D. L. Perrodin(2010), arXiv:1005.0634 [gr-qc].
 - [54] M. Levi, Phys. Rev. **D82**, 104004 (2010), arXiv:1006.4139 [gr-qc].
 - [55] J. Steinhoff, S. Hergt, and G. Schaefer, Phys. Rev. D **77**, 081501(R) (2008).
 - [56] J. Steinhoff, G. Schäfer, and S. Hergt, Phys. Rev. D **77**, 104018 (May 2008).
 - [57] J. Steinhoff, S. Hergt, and G. Schäfer, Phys. Rev. D **78**, 101503 (Nov. 2008).
 - [58] S. Hergt and G. Schäfer, Phys. Rev. D **78**, 124004 (Dec. 2008).
 - [59] R. A. Porto and I. Z. Rothstein, Phys. Rev. D **78**, 044013 (2008).
 - [60] R. A. Porto and I. Z. Rothstein, Phys. Rev. D **78**, 044012 (2008).
 - [61] A. Buonanno and T. Damour, Phys. Rev. D **62**, 064015 (2000).
 - [62] T. Damour, A. Nagar, E. N. Dorband, D. Pollney, and L. Rezzolla, Phys. Rev. D **77**, 084017 (2008).
 - [63] T. Damour, P. Jaranowski, and G. Schäfer, Phys. Rev. D **62**, 084011 (Sep 2000).
 - [64] J. W. York, Phys. Rev. Lett. **82**, 1350 (Feb 1999).
 - [65] H. P. Pfeiffer and J. W. York, Phys. Rev. D **67**, 044022 (Feb 2003).
 - [66] G. B. Cook, Phys. Rev. D **65**, 084003 (Mar 2002).
 - [67] G. B. Cook and H. P. Pfeiffer, Phys. Rev. D **70**, 104016 (Nov 2004).
 - [68] H. P. Pfeiffer, L. E. Kidder, M. A. Scheel, and S. A. Teukolsky, Comput. Phys. Commun. **152**, 253 (2003).
 - [69] <http://www.black-holes.org/SpEC.html>.
 - [70] L. Lindblom, M. A. Scheel, L. E. Kidder, R. Owen, and O. Rinne, Class. Quantum Grav. **23**, S447 (2006).
 - [71] H. Friedrich, Commun. Math. Phys. **100**, 525 (1985).
 - [72] D. Garfinkle, Phys. Rev. D **65**, 044029 (2002).
 - [73] F. Pretorius, Class. Quantum Grav. **22**, 425 (2005).
 - [74] C. Gundlach, J. M. Martin-Garcia, G. Calabrese, and I. Hinder, Class. Quantum Grav. **22**, 3767 (2005).
 - [75] O. Rinne, Class. Quantum Grav. **23**, 6275 (2006).
 - [76] O. Rinne, L. Lindblom, and M. A. Scheel, Class. Quantum Grav. **24**, 4053 (2007).
 - [77] J. M. Stewart, Class. Quantum Grav. **15**, 2865 (1998).
 - [78] H. Friedrich and G. Nagy, Commun. Math. Phys. **201**, 619 (1999).
 - [79] J. M. Bardeen and L. T. Buchman, Phys. Rev. D **65**, 064037 (Mar 2002).
 - [80] B. Szilágyi, B. Schmidt, and J. Winicour, Phys. Rev. D **65**, 064015 (Feb 2002).
 - [81] G. Calabrese, J. Pullin, O. Reula, O. Sarbach, and M. Tiglio, Commun. Math. Phys. **240**, 377 (2003), gr-qc/0209017.
 - [82] B. Szilágyi and J. Winicour, Phys. Rev. D **68**, 041501(R) (Aug 2003).
 - [83] L. E. Kidder, L. Lindblom, M. A. Scheel, L. T. Buchman, and H. P. Pfeiffer, Phys. Rev. D **71**, 064020 (2005).
 - [84] L. T. Buchman and O. C. A. Sarbach, Class. Quantum Grav. **23**, 6709 (2006).
 - [85] L. T. Buchman and O. C. A. Sarbach, Class. Quantum Grav. **24**, S307 (2007).
 - [86] D. Gottlieb and J. S. Hesthaven, J. Comput. Appl. Math. **128**, 83 (2001), ISSN 0377-0427.
 - [87] J. S. Hesthaven, Appl. Num. Math. **33**, 23 (2000).
 - [88] K. G. Arun, A. Buonanno, G. Faye, and E. Ochsner, Phys. Rev. **D79**, 104023 (2009).
 - [89] L. A. Gergely and Z. Keresztes, Phys. Rev. **D67**, 024020 (2003).
 - [90] E. Racine, Phys. Rev. **D78**, 044021 (2008).